Intraplate Volcanism In The Western Pacific Seamount Province

by
Matthew Ivan Sexton

A thesis submitted to the Earth and Atmospheric Sciences Department,
College of Natural Sciences and Mathematics
in partial fulfillment of the requirements for the degree of

Master of Science

in Geophysics

Chair of Committee: William W. Sager

Committee Member: Jonny Wu

Committee Member: Jim Gharib

University of Houston
December, 2021

ACKNOWLEDGMENTS

First, I'm extremely indebted to my advisor, Will Sager, for guiding me through the entire graduate process. Will has been unwavering in his support and is always willing to do whatever is best for his students. I want to thank the rest of my thesis committee, Jonny Wu and Jim Gharib, for their support as well. I want to thank the faculty at UH with who have help me develop through various classes and projects; especially: Yingcai Zheng, Hua-Wei Zhou, Rob Stewart, and Heather Bedle. I would also like to thank the UH staff for their assistance in navigating the UH bureaucracy; particularly, Jim Parker and Karen Maldonado, who are always cheerful and willing.

Indispensable to enduring grad school have been the many friends at UH who have provided help and advice, solidarity, and entertainment. Foremost is Sriharsha Thoram, who has been with me the whole time, and contributed in too many ways to count. From my first year, I have to thank Vaughn Robla, for helping me get started and having a backup when all my backups failed, and Rachel Clark, whose original research notes were very helpful. I am also grateful for the friendship shown by Walter Reed, Zhonghan Liu, Li Chang, Sharif Morshed, Dylan Weimer, Jackson Zerr, Andrea Paris, Carl Buist, Somaria Sammy, and Naila Dowla. I was lucky to be a part of two research cruises and I want to thank the crew and science parties on NBP 1808 and TN374 for making them valuable experiences, and my travel partners Benjamin Chang, Avradip Ghosh, and Malik Alam for being great companions on our various detours. Also thank you to Abdullah Alshangiti and Ibrahim Albeshr for all the coffee and all the great conversations.

I would like to thank my colleagues at Enervest: Bill Keller, Yoscel Shannon, Neil Shannon, Murari Khatiwada, Rene Mott, Livia Silva, Amber Peterson, Jorge Peinado, Victor Kriechbaum, Daniel Naval, and Jason Moore. I gained a ton of new perspective, and they were as supportive as anyone could possibly be. Finally, I am indebted to the Houston Geological Society and Society of Exploration Geophysicists whose financial support made this possible.

ABSTRACT

The Western Pacific Seamount Province (WPSP) is an area characterized by an abundance of large seamounts which are mostly Cretaceous aged and formed in an intraplate setting. The WPSP is located in an area with some of the oldest oceanic crust on earth, dating to the Jurassic in age. Understanding the volcanism in the WPSP has implications for the mechanisms of intraplate volcanism formation, timeline reconstructions of the Pacific Plate, and mechanisms for volcanism in deep ocean settings. I examine previous investigations into WPSP including ODP drilling investigations and reflection and refraction seismic surveys to understand the sediments, volcanic features, and crustal structure of the WPSP. We then compare these previous studies to interpretations from more recently acquired reflection seismic data to describe the age and stratigraphy of sediments in the WPSP.

It has been noted in previous studies the prevalence of igneous intrusions which permeate the subsurface in many areas of WPSP and in this study we examine in detail the structure and geometry, interaction with sediments, and emplacement mechanisms for such features in the seismic data. Our observations show that the geometries of igneous intrusions in deep ocean sediments are very different from what is observed in thick sedimentary basins, due to differences in the mechanical properties of the host rock. Thick sedimentary basins often cause intrusions to take the form of saucer-shaped sills and inclined sills, but this is not seen in the WPSP. We show that laccolith mounds are not uncommon and both laccoliths and sills can create volcanogenic vent complexes which can extend for 100s of meters upwards.

TABLE OF CONTENTS

LIST OF TABLES

LIST OF FIGURES

1. INTRODUCTION

The Western Pacific Seamount Province (WPSP) is an area located on the oldest part of the Pacific plate with Jurassic aged crust (Figure 1) (Müller *et al*., 2008). This area of the Pacific Plate is partially located in the Jurassic Magnetic Quiet Zone (JQZ), an area where the observed magnetic anomalies are small and hard to correlate making timeline reconstructions difficult (Figure 2). In the Mid to Late Cretaceous there were a number of widespread sporadic volcanic events that overlaid the Jurassic crust with volcanic intrusions and many seamounts of varying ages (Figure 3).

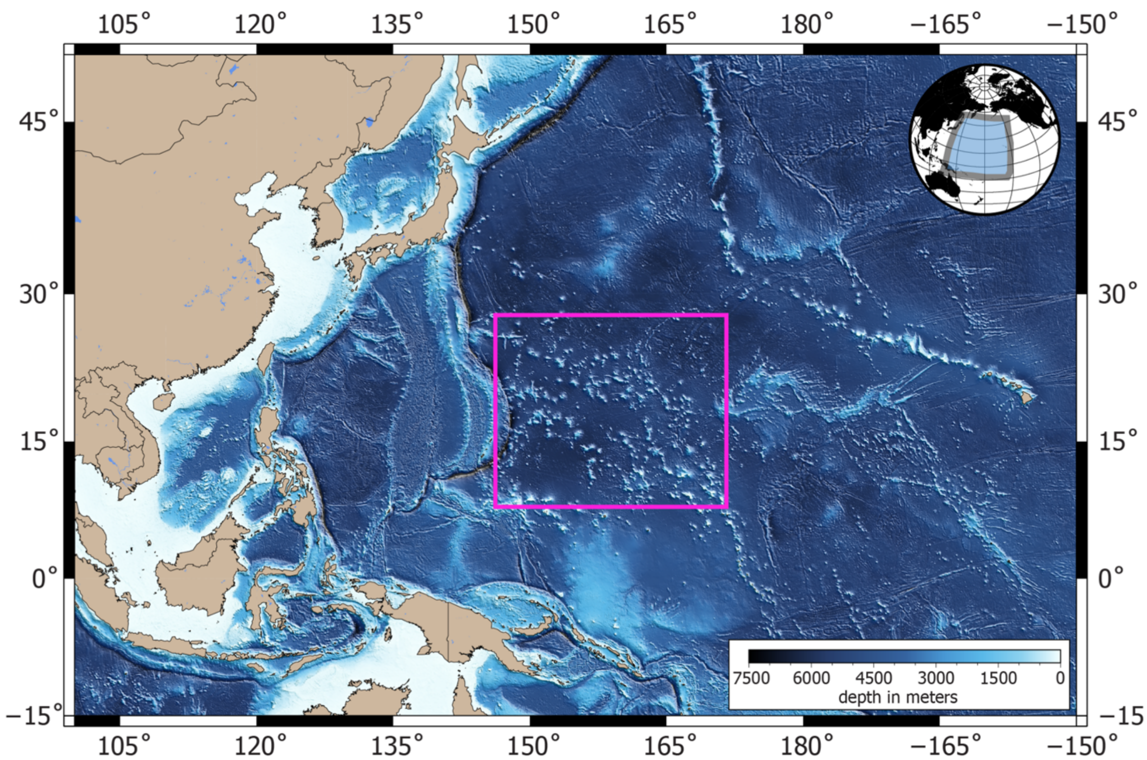

Figure 1. Bathymetry map showing the general study area with the WPSP outlined in pink (Data from Tozer et al., 2019).

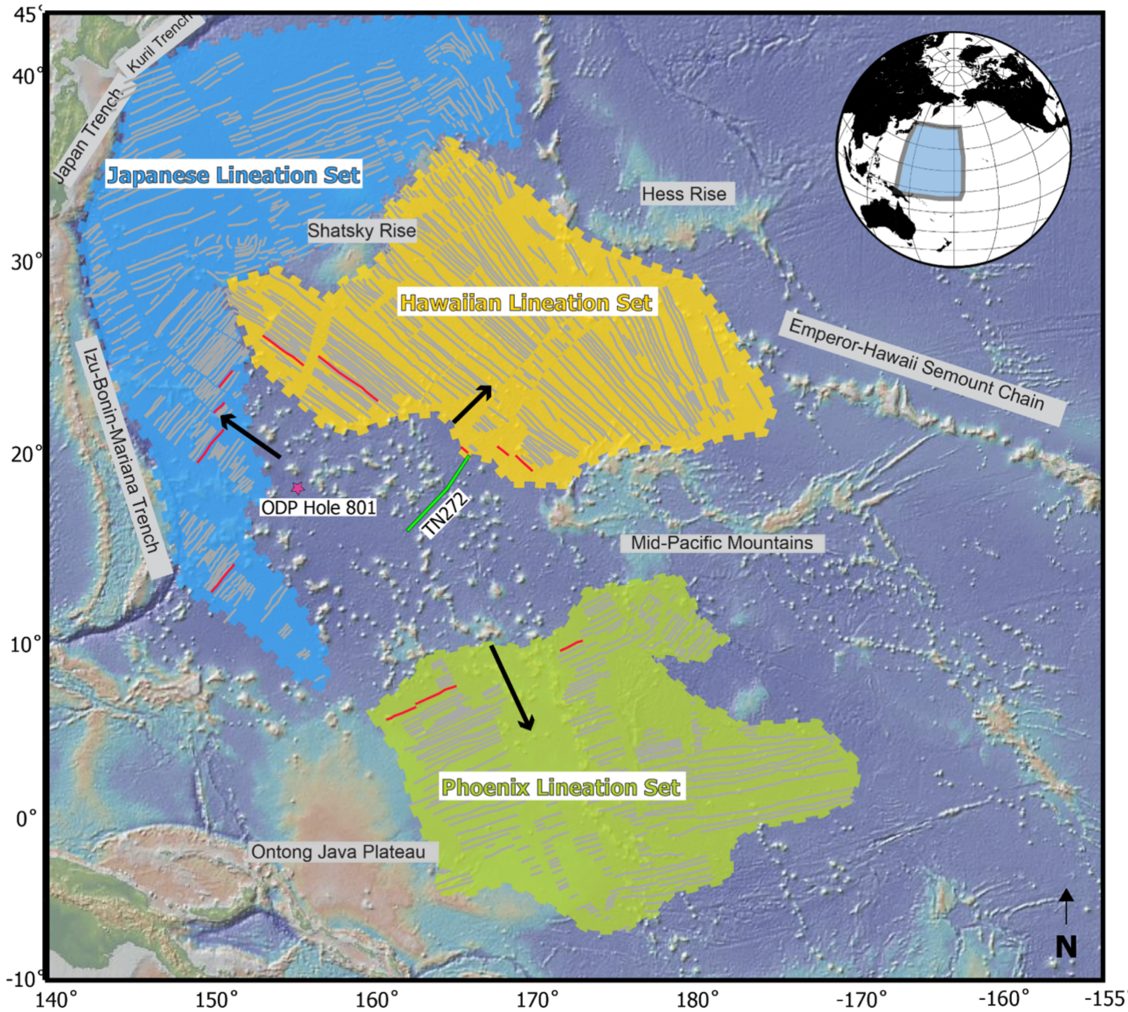

Figure 2. Map showing the Japanese, Hawaiian, and Phoenix magnetic lineation sets which outline the JQZ. Black arrows indicate the spreading direction of early Pacific plate. Grey lines are correlated magnetic anomalies. Red lines are the M29 magnetic anomaly which corresponds to ~157Ma. The green line represents the TN272 seismic survey track (Modified from Tominaga *et al*., 2015).

There are relatively few data of the subsurface in the WPSP. The Deep Sea Drilling Project (DSDP) from 1968-1983 made several attempts to drill into the Pacific plate in order to confirm and gather data on the Jurassic crust that were unsuccessful. The Ocean Drilling Program (ODP) attempted the same during ODP Leg 129 in 1989 and was ultimately able to drill into Jurassic crust at site 801 in Pigafetta Basin (Lancelot *et al*., 1990). The hole was revisited, and the basement rock logged in 1992 (Premoli Silva, *et al.,* 1993) and again in 1999, when the hole was deepened an additional 341m (Plank, *et al*., 2000). Several 2D seismic surveys were shot in the areas surrounding these ODP drill sites (MESOPAC II, FM35-12) which show the surrounding extent of the basement rocks and the sedimentary packages above which were characterized during ODP Leg 129 (Figure 4).

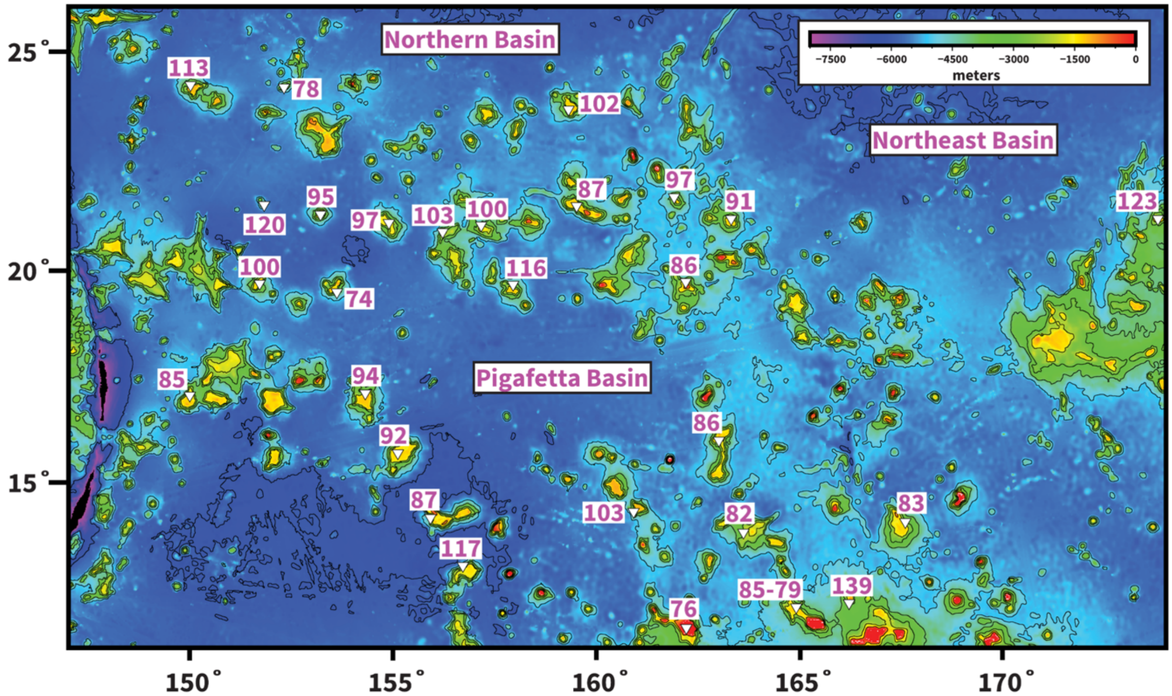

Figure 3. Map showing ages of seamounts in WPSP in millions of years. (Age data from Koppers, *et al*., 2003; Clouard & Bonneville, 2005; Yan, *et al*., 2021. Bathymetry data from Tozer *et al*., 2019)

Since 1989 two other seismic surveys were shot in the WPSP/JQZ region. One by the Japanese Coast Guard and Oceanographic Department in 2006 (survey MTr), included multi-channel seismic (MCS) lines in the northwest portion of the WPSP which surveyed over seamounts in the area. The data were analyzed by Stadler and Tominaga (2015) who observed the spatial distributions of the intrusions, their apparent ages based on the surrounding host rock, and concluded that they were of a similar age to the surrounding seamounts and fit the framework of the WPSP being formed as a result of small thermal upwellings originating from a deeper mantle source. More recently another seismic survey conducted by the National Science Foundation in 2011-12 (survey TN272) consists of a single ~800 km MCS line that was shot in the northeastern WPSP, in a corridor between seamounts. The following is an analysis of the TN272 MCS profile to determine the distribution and ages of the igneous intrusions and what these factors say about the formation of the WPSP. Although there are numerous studies using MCS data to show the structure and geometry of igneous intrusions in thick sedimentary basins, usually associated with hydrocarbon exploration, my study will show that the WPSP, being a deep ocean basin environment, displays a significant difference in the structure and geometry of igneous intrusions relative to sedimentary basins.

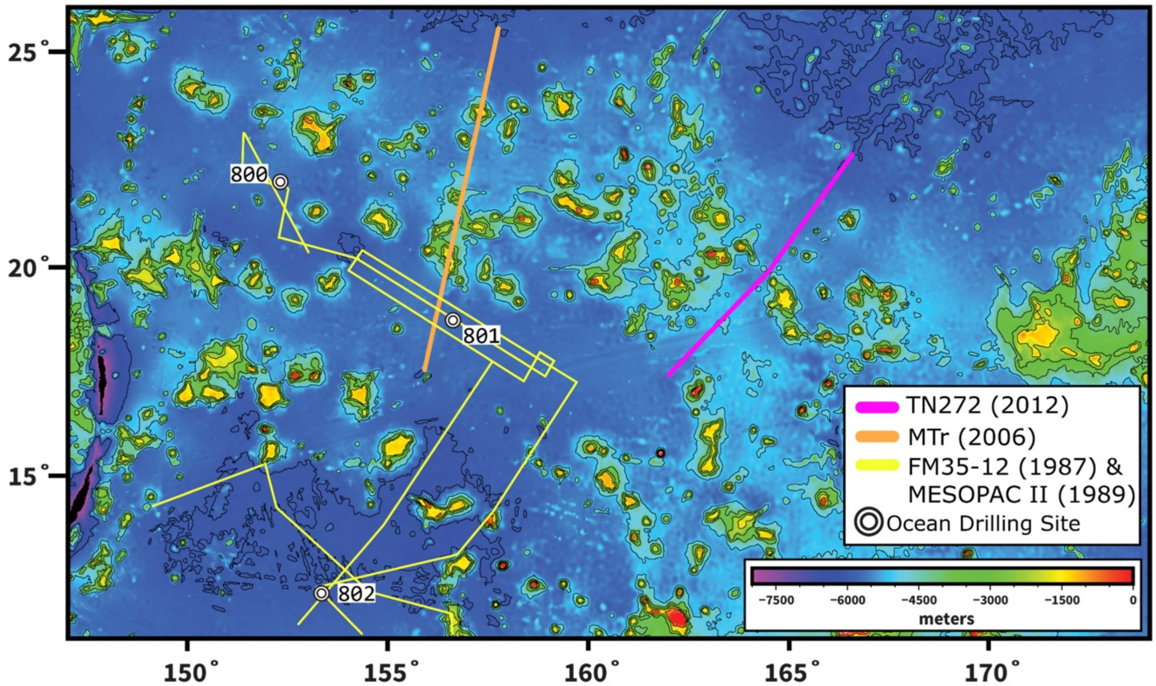

Figure 4. Multi-channel seismic surveys located in the WPSP (Bathymetry data from Tozer *et al*., 2019).

2. BACKGROUND

2.1 Geologic Framework of Western Pacific Intraplate Volcanism

The study of intraplate volcanism has been tied to the theory of a mantle "hot spot" for many years, but the idea of what a hot spot is has evolved to encompass a range of different models. The Hawaiian Islands and the Hawaiian-Emperor seamount trail were demonstrated to be the result of a hot spot possibly sourced in the deep mantle (Wilson, 1963; Morgan, 1971). Applying this model to other linear seamount chains is problematic. Courtillot *et al*. (2003) argue that only seven of 49 hotspots around the world can be explained by the Wilson-Morgan model and could be attributed to a deep mantle "primary plume". They classify other hot spots as the result of "secondary" thermal plumes, possibly originating from a "superplume", and "tertiary" hot spots which could have origins due to stresses in the lithosphere and decompression melting. Koppers *et al*. (2003) notes that the majority of seamounts in the WPSP fall under the secondary classifcation due to their geochemical composition and short seamount trail length. Contrasting mantle plume models are the "plate" class of models, which posit that shallow tectonic processes and mantle heterogeneities with low melting points as the cause of hotspots (Anderson and Natland, 2007). Simple evidence for the plate model is that most modern hotspots are located either near spreading centers or in intraplate settings which are extensional (Foulger, 2007).

The WPSP in the Western Pacific basin is located in the oldest part of the Pacific plate which was formed near the triple junction of the Phoenix-Farallon-Izanagi plates at ~180 Ma (Handschumacher *et al.*, 1988). The Pacific plate had a very high, half spreading rate of ~80 – 100 mm/year during the late Jurassic, which then slowed to ~30 – 50 mm/year in the early Cretaceous (Müller *et al*., 2008). Figure 5 shows a reconstructed timeline of the Pacific plate growth and how the WPSP was in the southern hemisphere near the equator in the Late Jurassic and during most of the Cretaceous. At ~85 Ma the plate motion changed to heading northwest and the WPSP eventually crossed the equator sometime after, during the Late Cretaceous, and finally migrated to its present location north of the equator. The paleodepth of the Pacific ocean is thought to have started at 2750 m at the Pacific-Farallon Ridge (Rea and Leinen, 1986; Rea and Lyle, 2005) and estimations from Van Andel (1975) indicate the area around the WPSP was at 3500 m in the Mid Cretaceous and 5500 m by the Late Cretaceous.

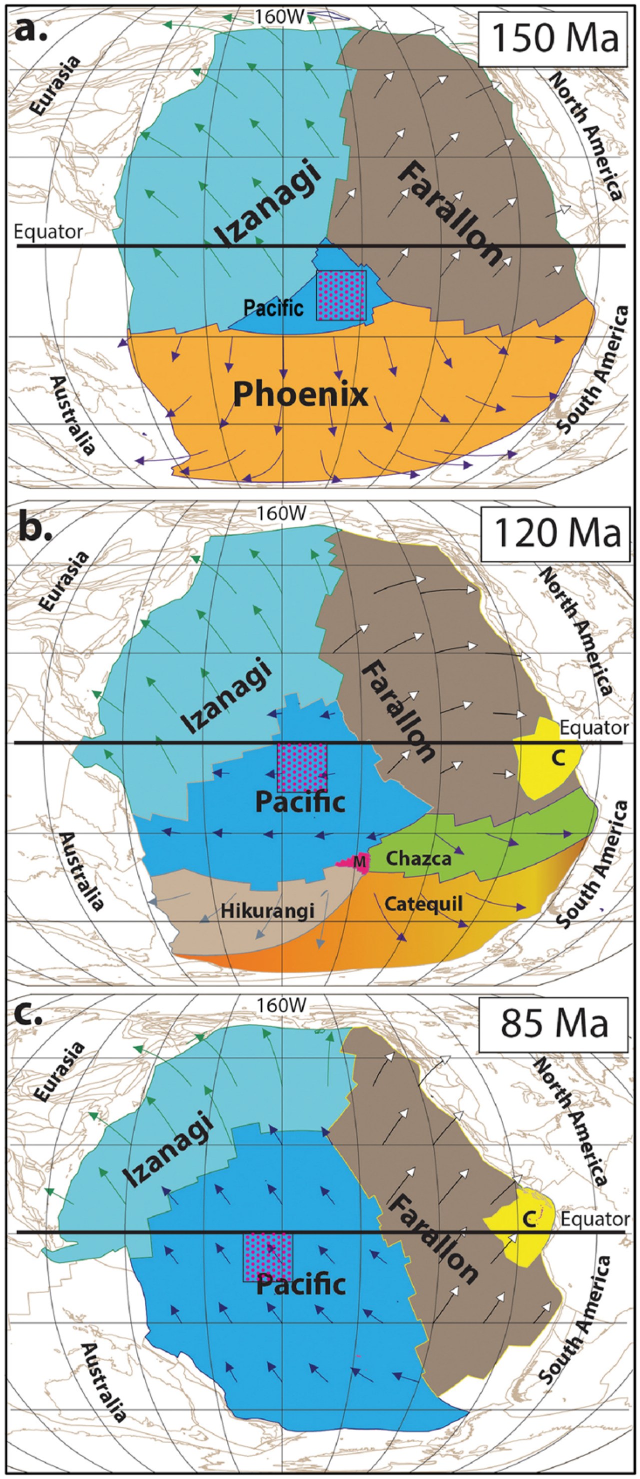

Figure 5. Reconstruction of the Pacific Plate at (a) 150 Ma – Late Jurassic, (b) 120 Ma – Early Cretaceous, (c) 85 Ma – Late Cretaceous. Pink dots highlight the WPSP location. Arrows signify plate motion vectors (Modified from Torsvik *et al*., 2019).

2.2 Scientific Ocean Drilling Results

ODP sites 800 and 801 were both drilled during Leg 129 in 1989 in Pigafetta Basin. Site 800 never reached the Jurassic crust, ending after reaching a Cretaceous doleritic sill at 544 meters below the seafloor (mbsf). Site 801 was drilled all the way to the Jurassic crust at 462 mbsf without encountering any Cretaceous sills. Table 1 shows a comparison of the sediment layers recovered at Sites 800 and 801, which can be summarized into 4 distinct sections (Lancelot, *et al*., 1990):

(1) pelagic brown clay, Cenozoic age;

(2) chert and porcellanite, deposited from Mid – Late Cretaceous;

(3) volcaniclastics, deposited from Early – Mid Cretaceous;

(4) radiolarite deposits, from Mid Jurassic – Early Cretaceous;

Table 1. Comparison between the ODP site sedimentary thicknesses and average sedimentary thicknesses from the TN272 MCS profile, measured in meters (m). Unit 5 shows the depth in meters below seafloor (mbsf).

	Site 800	Site 801	TN272 NE	TN272 SW
Unit 1	38m *Pelagic brown clay* Cenozoic	64m *Pelagic brown clay* Cenozoic	~72m	~44m
Unit 2	190m *Chert, porcellanite, & limestones* Campanian-Albian 72-112 Ma	63m *Chert and porcellanite* Campanian-Cenomanian 72-94 Ma	~115m	~71m
Unit 3	221m *Volcaniclastic turbidites & minor pelagic intervals* Albian-Barremian 112-128 Ma	191m *Volcaniclastic turbidites & minor pelagic intervals* Cenomanian-Albian 94-112 Ma	~135m	~114m
Unit 4	49m *Clays and radiolarite* Barremian-Berriasian 128-140 Ma	143m *Brown radiolarite* Valanginian-Bathonian 133-166 Ma	~170m	~104m
Unit 5 (Basement)	498mbsf *Doleritic Sill* Berriasian 140Ma	462mbsf *Basalt* Bathonian 166Ma	~492mbsf	~333mbsf

During ODP Leg 185, the hole at Site 801 was drilled 341m deeper into igneous basement (Plank *et al*., 2000).

A similar order of stratigraphic succession was found at Site 800, with the main differences being several limestone layers were observed within the Mid Cretaceous (94 – 112 Ma) section, indicating that there were sediment sources in the nearby WPSP that were above the carbonate compensation depth (CCD). Estimates of the CCD during the Cretaceous indicate a steady depth of ~4000 m (Van Andel, 1975; Lancelot *et al*., 1990), and it was expected that more carbonate sediments would have been observed in the recovered cores in Pigafetta Basin; especially in the older sediments when the ocean was shallower. It was postulated that a combination of crustal subsidence to a depth deeper than estimated and local fluctuations in the CCD, led to the lack of carbonate deposition (Lancelot *et al.*, 1990).

2.3 Previous seismic interpretations

There were 2 seismic surveys shot during the late 1980s, at and in the vicinity of ODP drill sites in Pigafetta Basin (MESOPAC II, FM35-12). Abrams *et al*. (1992, 1993) used the information from ODP Leg 129 to make interpretations of these seismic lines and were able to correlate them with the sedimentary records at ODP Sites 800 and 801. In addition to mapping the sedimentary sections, a difference was noted in seismic characteristic of underlying basement as being either “rough” or “smooth”. They posited that the “rough” basement corresponds to areas where the Jurassic crust is exposed to the overlying sediments and “smooth” a result of doleritic sills overlying the Jurassic crust. A “rough smooth boundary” (RSB) was mapped where this transition from rough to smooth was noted.

Kaneda *et al*. (2010) described the crustal structure of the northern WPSP using refraction seismic data from the MTr survey line which passes very near ODP Site 801 (Figure 4). Using tomographic inversion they created a p-wave velocity model outlining the crustal thicknesses. Based on these velocities they interpret the crust in Pigafetta Basin to be 7.5 – 8.0 km thick and in the northern basin to be 6 km thick. Studies synthesizing oceanic crustal thickness (Christeson *et al.,* 2019; Van Avendonk *et al.,* 2017) have shown average thickness to be ~6 km which would make Pigafetta Basin anomalously thick; however, they also show that there is a positive correlation between crustal age and thickness, which might explain the anomaly. Moho depth was calculated to be at 14 km in Pigafetta Basin and 12 km in the basin farther north.

Underneath the seamount clusters, the crust thickens to a maximum of 16 km with maximum Moho depth at 19 km. Kaneda *et al.* (2010) contend the increased Moho depth is mainly due to plate flexure, but also partially due to the increased crustal thickness from igenous intrusions. They also noted that the seamount structures consisted of a relatively small intrusive core and that the preponderance of the seamount volume is a result of erupted lavas and volcaniclastics.

Stadler and Tominaga (2015) mapped volcanism in the Pigafetta Basin using MCS data from the MESOPAC II, FM35-12, and MTr surveys. They focused on mapping the sedimentary packages and interpreted volcanic features, both intrusive and extrusive. They inferred the intrusive volcanic features in Pigafetta Basin to be of similar ages to the surrounding seamounts and noted that the spatial distribution of volcanic features are nonsystematic. They interpreted that these two observations suppport the hypothesis of a large superplume beneath the WPSP from which many smaller plumelets rose into the crust. They also argue that the RSB described by Abrams *et al*. (1993) is caused by different modes of late stage volcanism causing different expressions rather than signifying Jurassic crust or Cretaceous sill.

2.4 Igneous intrusions in seismic data

Sills and dikes are tabular, sheet, igneous intrusions that commonly intrude sedimentary rocks. They can also intrude into crustal rocks and pre-existing lava flows, though this is less commonly observed in seismic data due to the low impedance contrast between the intrusive body and the host rock (Á Horni *et al*., 2017).

Dikes typically propagate vertically to sub-vertically in the direction perpendicular to the minimum total stress of the surrounding rock or invade areas of weakness such as beddings planes and fractures (Gonnermann, 2015). Dikes can exist as conduits from a magma chamber and serve as vertical piping throughout the subsurface magma complex and can form feeder dikes that allow magma to the surface. They can also form structures called ring dikes that have concentric circular patterns on top of a magma chamber after a magma chamber has drained (Lockwood and Hazlett, 2010).

Sills commonly form horizontal sheets parallel to sedimentary bedding planes (Kavanagh *et al.,* 2006; Lockwood and Hazlett, 2010). Though they are dominantly layer parallel, in local sections they can cut across layers, may exhibit holes, and can split or merge with adjacent sills (Planke *et al*., 2005). Traditionally it was thought that dikes dominated the vertical piping in a subsurface magma complex, but more recent evidence from reflection seismic data has shown that this is not always the case. Numerous interconnected inclined sills, which are not flat-lying, have been shown to facilitate magma flow for distances up to 12 km vertically, without dikes as a primary conduit (Magee *et al*., 2016).

While the layer parallel sill is the most common geometry, there are other geometries documented in seismic data. Different geometries can imply a geologic setting and parameter constraints of the host rock and intruding magma. Sills, like dikes, can intrude into zones of weakness that can be due to lithology, fractures, or unconformities and bedding discontinuities. Kavanaugh *et al*. (2006) suggest that rigidity contrasts also play a role in determining the stratigraphic boundary at which a sill intrudes. They showed experientially that with two layers of similar density but high rigidity contrast, the sill will intrude in a plane below the more rigid layer. There are examples of this occurring when sills intrude below a previously emplaced sill (White *et al.*, 2012) and below rigid sandstones (Hyndman and Alt, 1987).

There are several different sill geometries that have been documented in seismic data (Figure 6), and there are key differences in what causes these differing geometries to form. A layer parallel sheet (Figure 6A) typically occurs when the magma follows along stratigraphic boundaries and also is common in soft sediments (Magee *et al*., 2015; Planke *et al*., 2005). A saucer-shaped sill (Figure 6B) is a common morphology when the surrounding rock has elastic strength. It is thought that this shape develops after sills reach a critical size where a difference in stress at the sill edges allows them to transgress sedimentary layers (Malthe-Sørenssen *et al*., 2004; Planke *et al*., 2005). Stair-step sill geometries (Figure 6E) are shown to occur when magma follows sub-vertical fractures and also can form at the transgressive edges of saucer-shaped sills in conditions where the host rock is brittle (Schofield *et al*., 2012). In addition, Schofield *et al*. (2012) show that the direction of magma flow can be inferred from these step morphologies. Magma fingers (Figure 6F) have been shown to occur in non-brittle, low strength, host rock where the host rock

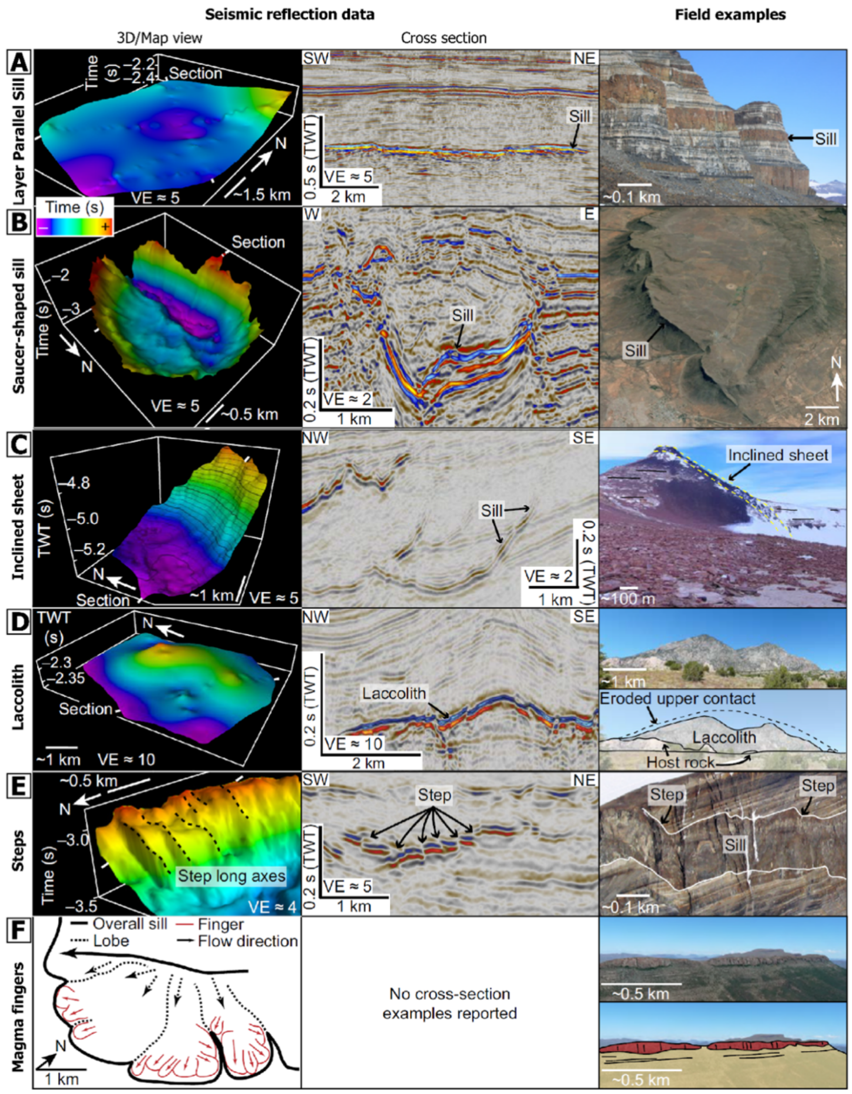

Figure 6. Examples of different sill geometries observed in reflection seismic (Modified from Magee *et al*., 2014, 2015).

behaves in a ductile fashion, deforming along the magma front and creating a viscous-viscous interface where the host rock behaves as a fluid, leading to globular fingers (Magee *et al*., 2019; Poppe *et al*., 2019; Schofield *et al*., 2012). Sills can have either bilateral or radial symmetry or can form a more complex hybrid of both (Thomson and Hutton, 2004); Kavanagh *et al*., 2006). More complex structures form over time as igneous activity is often incremental and protracted, and deformation from initial intrusions can lead to later intrusions as the host rock is less homogenous (Magee *et al*., 2016). The size of sills complexes can vary greatly with large sills extending hundreds to thousands of square km with thicknesses most commonly on the order of 50-150 m, whereas smaller sills may only extend a few square kilometers (Francis, 1982;

Kavanagh *et al*., 2006; Magee *et al*., 2015). Laccoliths (Figure 6D) are sill-like intrusions that are dome or lens shaped (Lockwood and Hazlett, 2010). Walker *et al.* (2020) show that larger domed laccolithic structures can be an amalgamation of smaller interconnected sill-like intrusions that build up over time.

3. METHODS

Seismic data

The TN272 seismic data were acquired in 2011 on the R/V *Thomas G. Thompson* and consists of a single line ~800 km long and one crossline of ~57 km length. It was acquired with 2 GI guns as a source with a 48-channel streamer as a receiver. The receiver spacing was 12.5 m and the shot spacing was 25m. The CDP bins were 6.25m for a fold of 12. The data were post stack time migrated using Memory Stolt F-K migration using ProMAX software. The dominant frequency is 60 Hz which gives a vertical resolution of about 8 – 10 m using an average velocity of 2000 m/s, a reasonable average velocity for deep sediments. The polarity of the data is shown such that a downward increase in acoustic impedance will result in a positive amplitude (Figure 7).

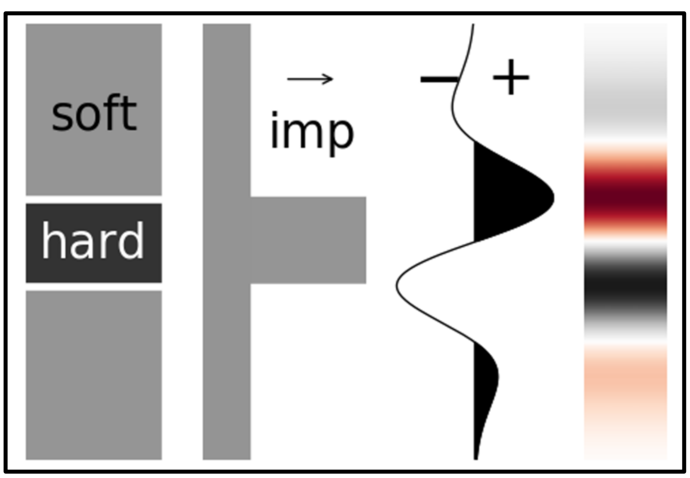

Figure 7. Polarity convention of the TN272 MCS seismic data

Bathymetry data

High-resolution multibeam bathymetry was collected along the TN272 seismic line using a Kongsberg Simrad EM302 30 kHz multibeam echo sounder. In addition, multibeam data from 16 other bathymetry surveys were combined to make a regional high-resolution map of the area surrounding TN272

Table 2. List of multibeam bathymetry surveys used for high resolution bathymetry maps.

SURVEY NAME	YEAR	TRACK LENGTH (Km)
SR1906	2019	743
EX1607	2016	269
EX1606	2016	938
EX1604	2016	4241
RR1612	2016	724
SKQ201402S	2014	2120
MV1301	2013	745
KM1226	2012	744
MGL1202	2012	114
TN272	2011	2105
EX1005	2010	767
EX1003	2010	808
KM1004	2010	715
KM0913	2009	793
AHI-07-01	2007	89
HI-07-01	2007	31

(Table 2). The data were processed by applying heave, pitch, and roll sensor corrections and a combination of automatic and manual filtering techniques to remove erroneous soundings using CARIS software. A single regional surface was created from the aggregate of these high-resolution surveys with 100 m grid spacing. Finally, the high-resolution surface was combined with a grid of low-resolution, satellite altimetry derived bathymetry data, to fill in data gaps (Tozer *et al*., 2019).

Gravity data

Gravity anomaly data were extracted from the satellite altimetry derived gridded gravity data by Sandwell *et al.* (2014).

Seismic interpretation methods

In order to interpret the seismic data, seismic facies analysis was performed using seismic stratigraphy methods (Mitchum *et al.,* 1977) which examine reflector continuity, configuration, amplitude, and frequency to interpret seismic signatures as geologic features. Sills were identified as reflectors with the following criteria in order of importance: (1) very high relative amplitude; (2) abrupt terminations; (3) attenuation of signal below reflector; (4) low frequency; (5) continuous, (See Figure 8 for an example of sill seismic signature). Criteria 1 – 3 have to do with the manifestations of the physical nature of sills in seismic data, whereas 4 – 5 are about increasing the probability of a reflector being signal and not noise. The identified sills were then classified under one of the geometries in Figure 6.

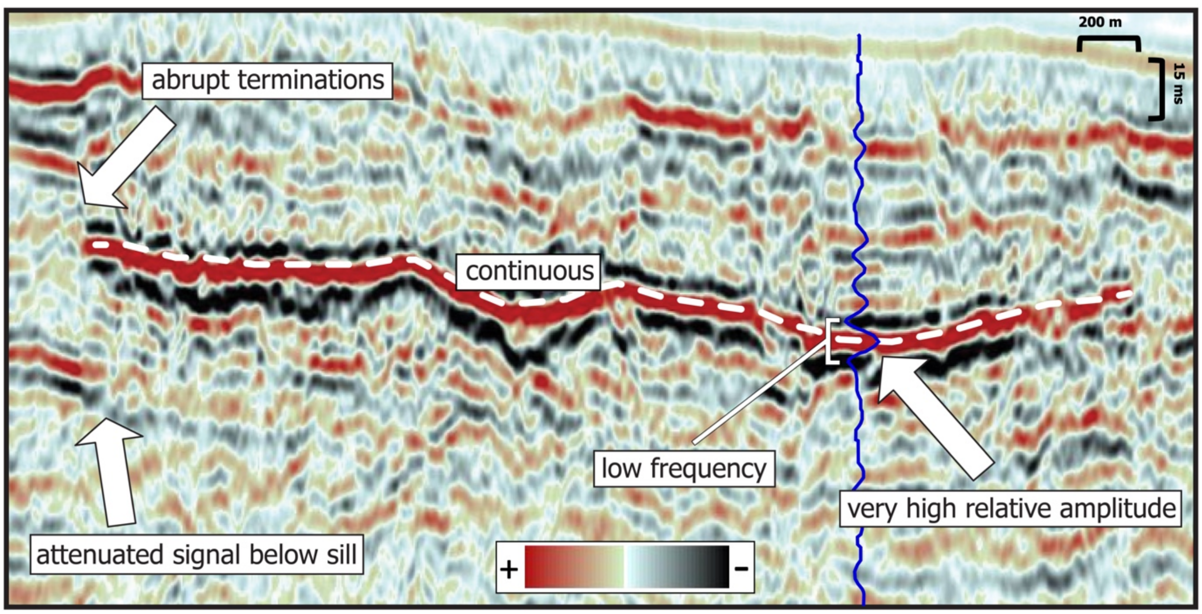

Figure 8. Example of a sill from the TN272 seismic amplitude data showing the characteristics used to classify a sill. The blue line shows one of the stacked seismic traces that make up the image. Image color represents the degree of positive (red) or negative (black) amplitude of the seismic trace signal (See Figure 6 for polarity convention)

4. RESULTS AND INTERPRETATIONS

4.1 Regional observations

For survey TN272, the depth to the seafloor (Figure 9A) starts at around 5600 m in Pigafetta Basin on the SW end of the line. From there, depth decreases for 225 km to a topographic high point at 5100 m, and then gradually deepens for the next 575 km to a depth of 5900 m in the basin NE of the seamount chains. This latter basin is overall a deeper basin than Pigafetta Basin. The gravity anomaly derived from satellite altimetry (Figure 9B) typically mirrors seafloor topography; however, there are two notable deviations. There is a trough of several hundred mGal from 250 – 500 km and another trough, ~100 mGal, from 675 – 750 km. The deviation from the seafloor topography was noted by Feng (2016) as being due to the survey passing through gravity moats caused by the nearby seamounts, which can be seen in the regional 2D gravity anomaly grid (Figure 10). The 500 km trough is also enhanced by the fact that preceding it is a broad swell in the bathymetry and in the gravity data, from 100 – 400 km. The gravity grid shows that this broad swell extends nearly 300 km to the SE and doesn't appear on the surface to be directly connected with any of the surrounding primary seamounts.

Figure 9. Series of data profiles along the TN272 seismic survey track with the horizontal axis denoting distance along survey in km. **(A)** Depth to seafloor (m), **(B)** Gravity (mGal), **(C)** Reflection seismic TWT (s), **(D)** Reflection seismic with major horizons mapped, **(E)** Reflection seismic overlain with velocity model from Feng (2016) derived from sonobuoy refraction data. Left axis is TWT (s) and right axis is depth from sea level (km). The black lines are iso-velocities and the colored lines highlight a sudden velocity change. See original velocity model for velocity values (Modified from Feng (2016)), **(F)** Original velocity model from Feng (2016). Depth and distance are in km. Velocities are represented by color and range from 1.5 – 8 km/s

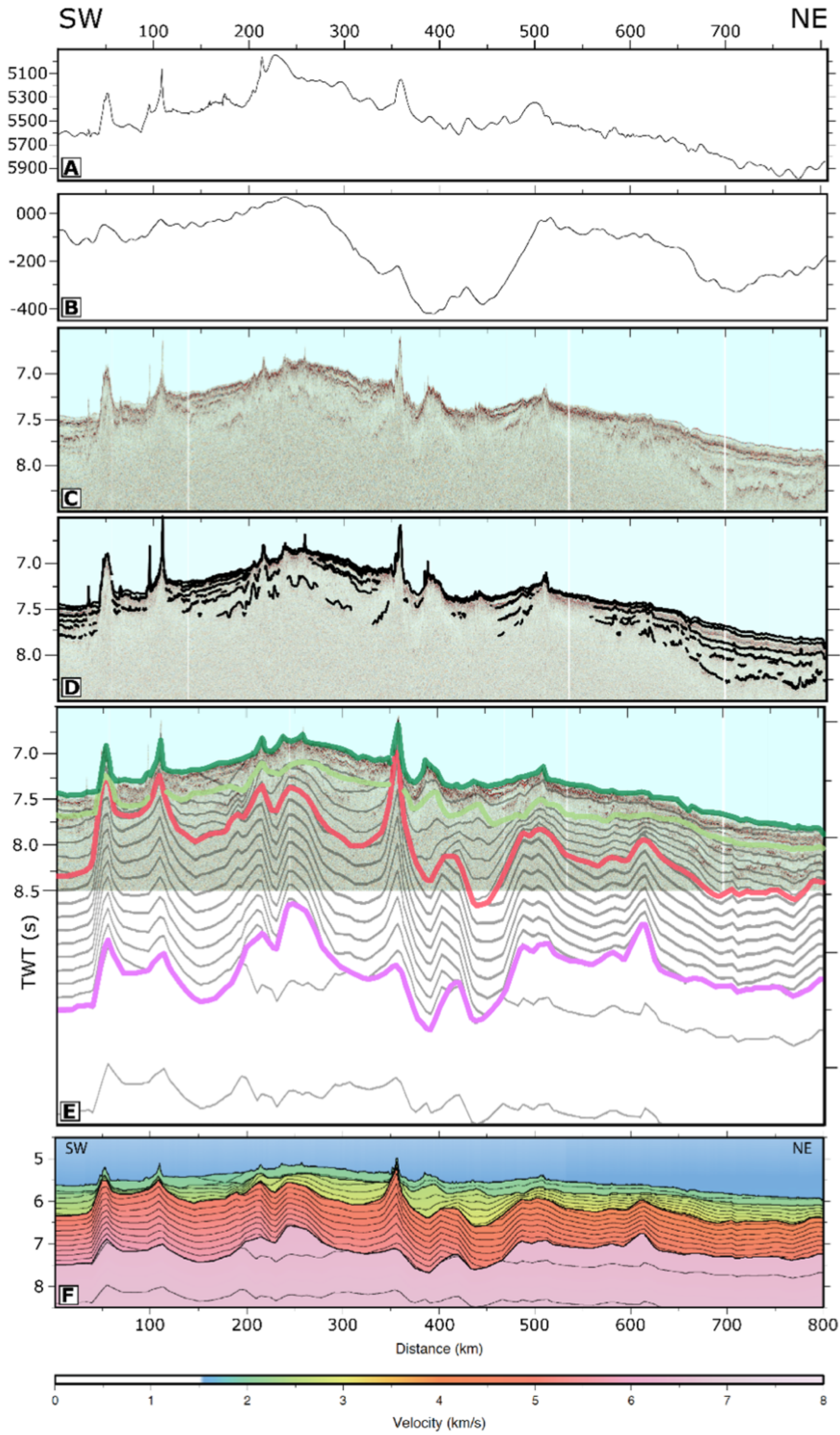
SW
NE
100
200
300
400
500
600
700
5100
5300
5500
5700
5900
Depth (m)
A
000
-200
-400
Gravity (mGal)
B
7.0
7.5
8.0
TWT (s)
C
D
8.5
TWT (s)
5
6
7
8
Depth (km)
E
SW
NE
F
Depth (km)
800
Distance (km)
0
1
2
3
4
5
6
7
8
Velocity (km/s)

The reflection seismic profile (Figure 9C) with the major horizons mapped (Figure 9D) shows four sedimentary units and the deepest horizon represents the beginning of basement rock. Beginning from the SW end of the line, all four units are present with a total thickness of about 0.6s TWT which continue with some interruptions until 200 km. At that point there is a facies change and the number of significant, mappable, horizons decreases and become shallower aside from one deeper reflector. This area of lesser continuity, beginning at 200 km, continues until ~600 km where we again see 4 units which thicken to 1.0s TWT.

Feng (2016) used sonobuoy refraction data from the TN272 survey to create a velocity model (Figures 9E and 9F). The velocity model highlights four velocity horizons, all which correspond to a rapid velocity increase. Feng (2016) interpreted the dark green horizon as the beginning of the sedimentary rock and the subsequent light green horizon below, as more compacted sedimentary rock with many igneous intrusions. The red line was interpreted as the beginning of Jurassic basement rock, and the final pink line indicates a velocity change below the shown reflection seismic record.

We can compare this velocity model interpretation with the reflection seismic profile. In the SW end 0 – 40 km segment, there is a significant difference in the velocity model interpretation of Jurassic basement and acoustic basement in the reflection seismic. Using the reflection seismic scale, the difference is ~0.5 s TWT. This is evidence that the acoustic basement in this segment is not Jurassic basement but instead overlying intrusive sills.

The 40 – 350 km segment has two areas of thick sedimentation which the velocity model suggests are highly intruded and compacted. There are also a number of prominent seamounts in this segment. The largest seamounts, located at 40, 110, and 350 km, all appear to have an intrusive core, evidenced by the increased, basement-level, velocities. The smaller seamounts, located from 210 – 260 km, do not appear to have this intrusive core, indicating they are composed primarily of erupted extrusive material. From 350 – 550 km the velocity model indicates a thick sediment basin, which we do not see much in the reflection seismic. The seamounts at 400 and 510 km don't exhibit an intrusive core in the velocity model and again

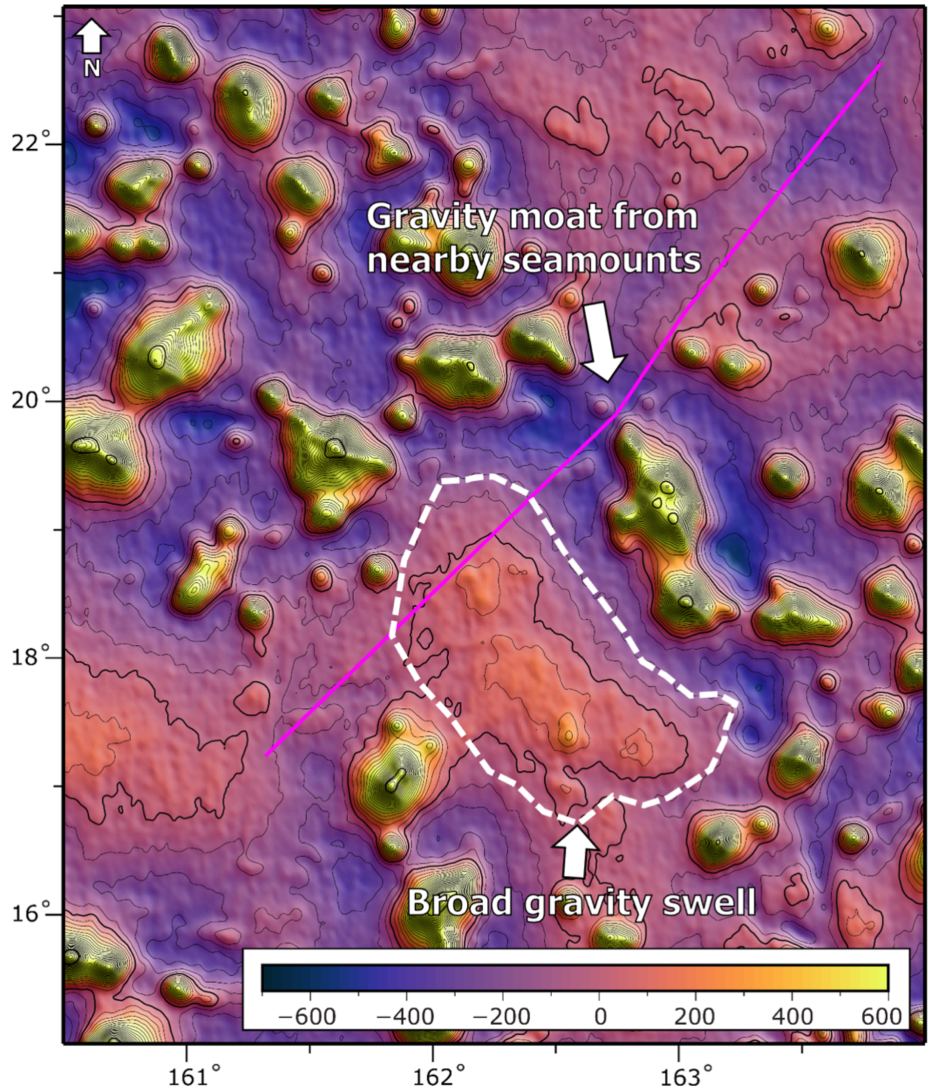

Figure 10. 2D gravity (mGal) grid of the area surrounding TN272 survey (Data from Sandwell, et al.; 2014). Pink line represents the TN272 seismic survey track.

probably extrusive. The extrusive material appears to extend to a wider area around the seamount than those in the previous segment evidenced by the lack of visible sediments in the reflection seismic for large distances in this segment. There are sediments visible from 450 – 490 km, and the sharp slope of the basement in the reflection seismic agrees with structure in the velocity model showing a thick sedimentary basin, albeit to a lesser degree. The segment from 550 – 800 km again shows another sedimentary basin, seen both in the velocity model and the reflection seismic.

The regional bathymetry surrounding TN272 (Figure 11) shows the range of volcanic features that are expressed on the seafloor. For reference, the features can be divided into three groups: primary, secondary, and tertiary seamounts, based on size. Primary seamounts are large enough to be easily visible with only the satellite bathymetry. Secondary seamounts are medium sized and are only slightly visible in the satellite bathymetry with the exact shape being unclear. Tertiary seamounts are the smallest seamount

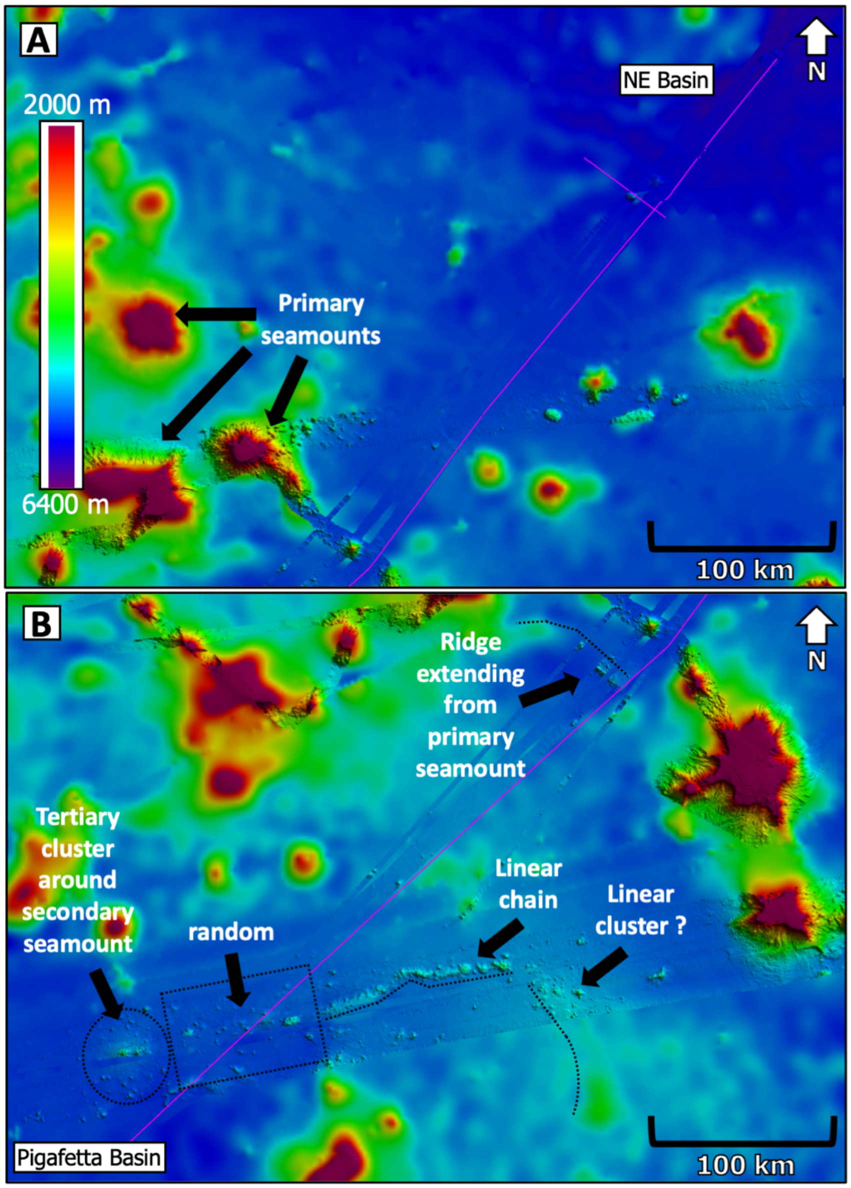

Figure 11. Regional multibeam bathymetry (in meters) surrounding the (A) NE half of TN272 seismic survey. (B) SW half of TN272 seismic survey. Black arrows indicate highlighted volcanic features. and the pink line represents the TN272 seismic survey track.

cones, only visible in locations where there is multibeam bathymetry data. The data show that the SW half of the survey line has more secondary and tertiary volcanic features the NE half, which extends past the northern boundary of the WPSP. Some of the secondary features are directly connected to the primary seamounts, such as the NW-SE trending ridge in Figure 11, which rises towards the primary seamount to the NW. The features not apparently connected to one of the primary seamounts display a number of different spatial distributions including single clusters, linear clusters, linear chains, and random distribution.

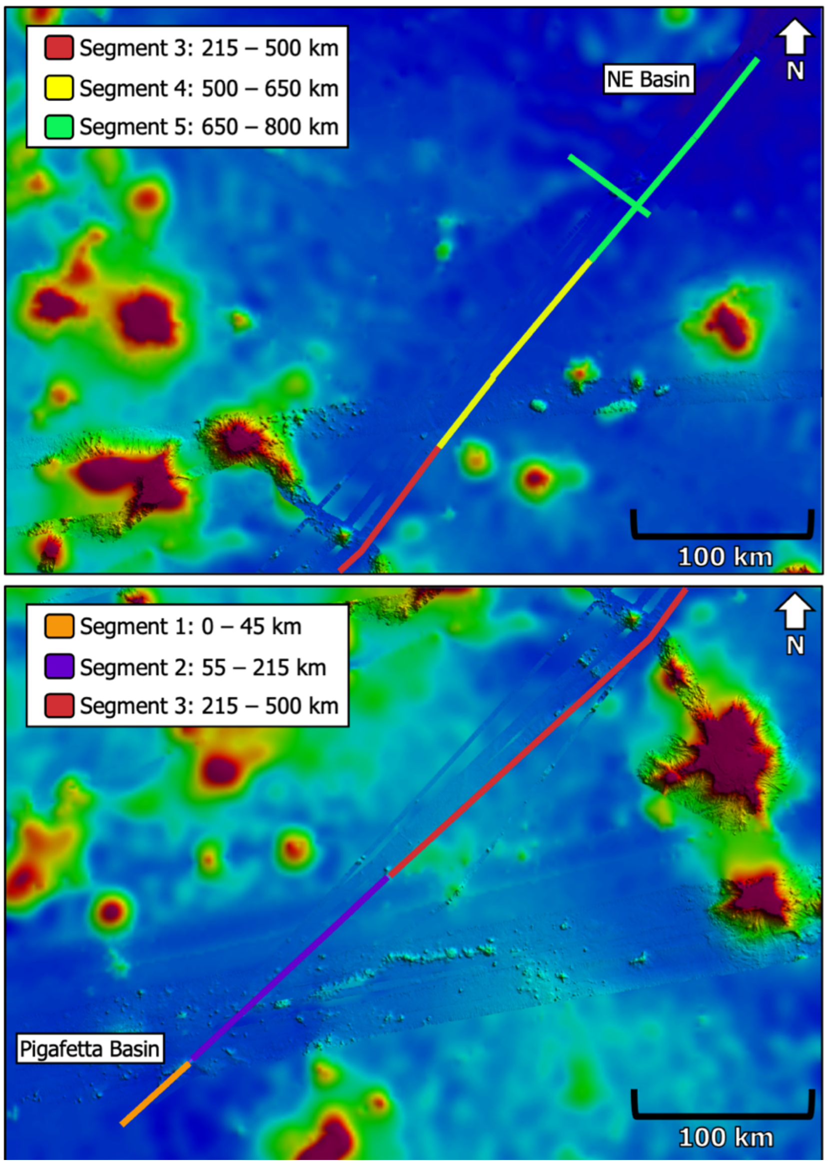

Figure 12. Segments of the TN272 seismic profile to be shown starting with segment 1 in Pigafetta Basin. Regional bathymetry scale is the same as Figure 11.

4.2 Seismic Profile

The TN272 seismic profile was separated into different five different segments for presentation (Figure 12). The SW segment, located in Pigafetta Basin, three middle segments passing over seamounts and areas of heavy surface volcanism, and the segment of the profile located in the NE basin. Four different sedimentary "units" were mapped using seismic facies analysis (See Figure 13 for example). In addition to the seismic facies, three horizons were mapped as well. A seafloor horizon, a high amplitude reflector in Unit 2 called "Horizon C", and an acoustic basement horizon that represents the deepest visible reflectors. The igneous features were then mapped and identified as sills if they fit the stated criteria listed in the methods (ex. Figure 8). Additionally, there were a number of vertical anomalies with chaotic reflections which were labeled Vertical Disturbed Zone(s) (VDZ), and which are interpreted as being either poorly imaged domed laccoliths or volcanogenic vent systems (Jackson, 2012; Stadler and Tominaga, 2015).

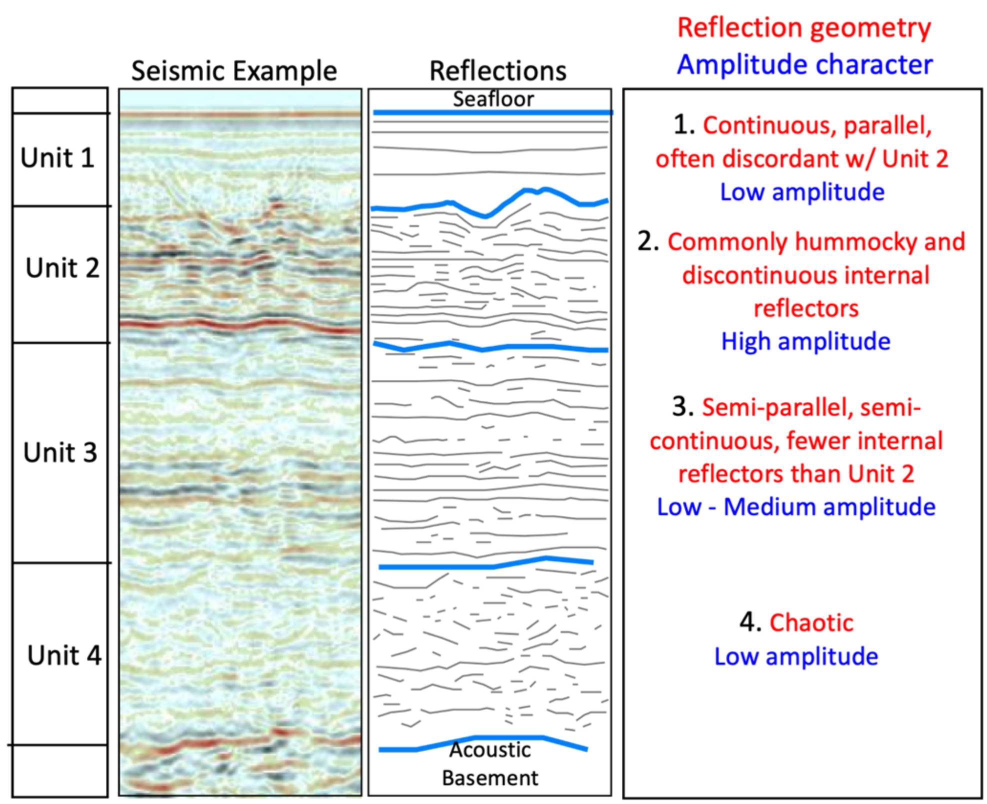

Figure 13. Example seismic facies of mapped sedimentary units 1-4.

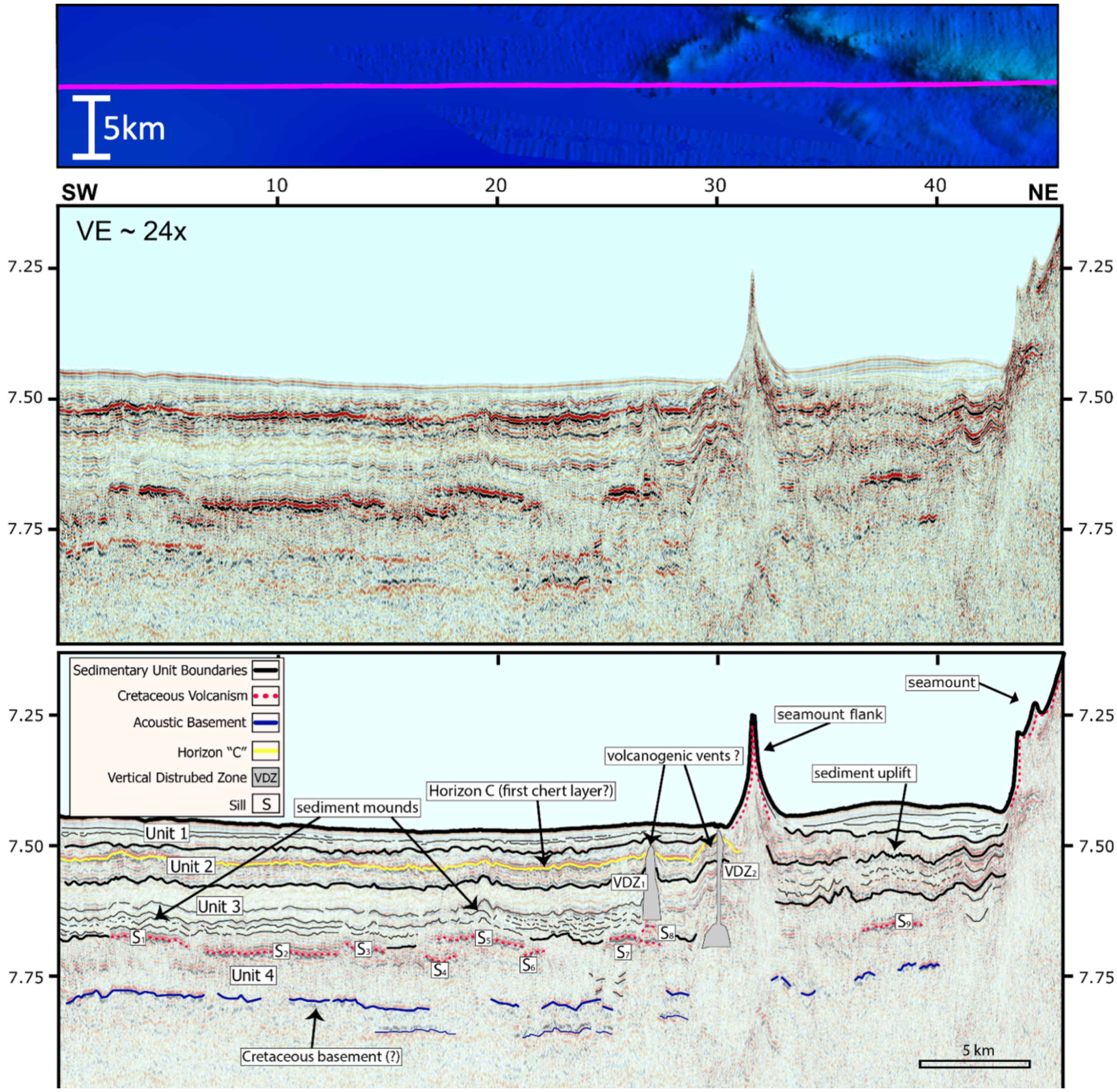

Figure 14. Segment 1 of TN272 seismic line located in Pigafetta Basin. Above: Local bathymetry in meters (m) along TN272 seismic line (pink). Below: Original and annotated reflection seismic profile with two-way-traveltime (TWT) on the vertical axis in seconds (s) and distance in kilometers (km) on the horizontal axis. Seismic amplitude scale is the same as in Figure 8. Bathymetry scale is the same as Figure 11.

Segment 1, Pigafetta Basin, 0 – 45 km

The seismic data in Segment 1 (Figure 14) has four distinct seismic facies. At the top, Unit 1 is a thin sequence with low amplitude that is either flat-lying on or onlapping the unit below. Unit 2 is a relatively high amplitude sequence that contains a large continuous high amplitude reflector, horizon "C", and is interpreted as the beginning of the chert sequences found at Sites 800/801. The top of Unit 2 is discordant with Unit 1, and has internal reflectors that are discontinuous and hummocky. Unit 3 is a lower amplitude unit with semi-continuous, semi parallel layers which are concordant with the Horizon C in Unit 2. The upper half of Unit 3 is characterized by low frequency reflectors and the lower half by higher frequency reflectors. The boundary between Unit 3 and 4 is marked by numerous high amplitude reflectors of low frequency that terminate abruptly, which are interpreted as intrusive sills. They are marked with an "S" and numbered sequentially along the seismic profile. Unit 4 is an entirely chaotic transparent unit with almost no visible continuous bedding planes. At the base of Unit 4, at 7.8s TWT, is acoustic basement that consists of a semi-continuous, medium amplitude reflector. There are also a couple of deeper lying reflectors below basement seen at 15, 24, and 27 km that have a reversed polarity.

There are 9 sills identified in this section, all of which are layer parallel. From 0-8 km there are two reflectors that can be seen which could be classified as sills due to their abrupt terminations, but they are much weaker in amplitude and there are not enough visible sediment layers around to compare amplitude. S_1 – S_3 all intrude on the same sedimentary interface between Unit 3 and 4. The group of S_4 – S_6 are an example of a stacked sill complex, as is S_8 and S_7. Sediments above the sills are frequently disturbed. S_1 and S_5 have multiple sediment mounds above them and the sediments above S_9 display a broad uplift.

At 27 and 30 km there are chaotic facies with a vertical trend that cross-cuts horizontal reflectors which are labeled VDZ 1 and 2 and which are interpreted as possible volcanogenic vents. Looking more closely, Figure 15A shows that VDZ_1 is directly above the S_7/S_8 stacked sill complex. The volcanogenic vent is ~500 m wide and it appears to have disturbed sediments and caused a forced fold up through Unit 2 with the Unit 1 sediments onlapping the mound. In addition, there are normal faults observed on the flank of the fold. Figure 15B shows a different type of vertical structure. The volcanogenic vent is ~200 m wide and there is no observed underlying sill. Instead, there is an underlying mound structure with chaotic facies which is directly located adjacent to a seamount flank and is interpreted to be an intrusive laccolith. A number of reverse faults occur on the SW side of the fold. The seamount flank with the nearby vent, can be seen in the bathymetry profile (Figure 14) to be part of a linear seamount trending NE of the seismic profile. The other seamount in the profile at 45 km is an even larger linear seamount trending perpendicular to the first one.

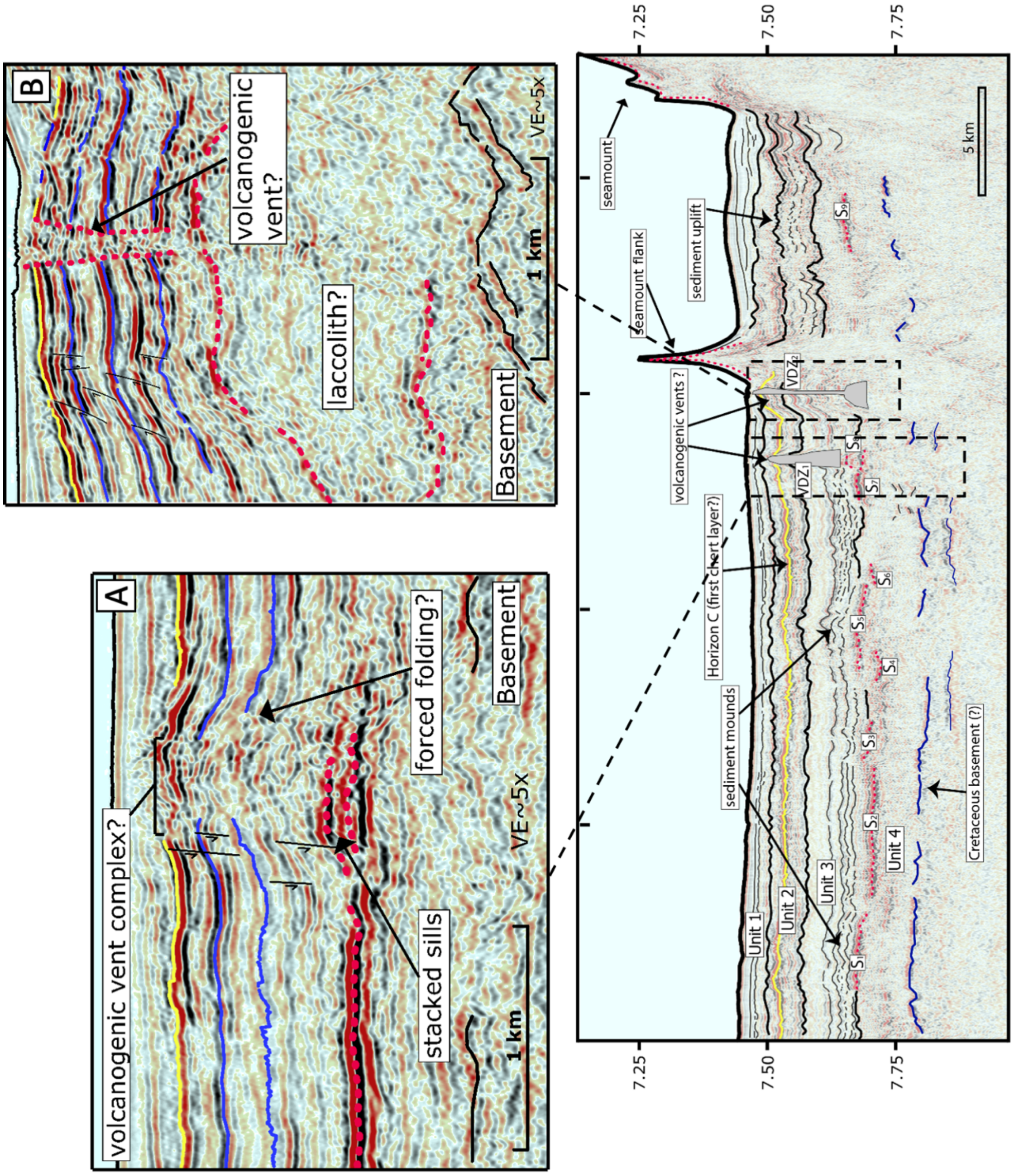

Figure 15.Close-ups of (A) VDZ 1 and (B) VDZ 2 from segment 1 in Pigafetta Basin (amplitude scale is the same as in Figure 8).

Segment 2, 55 – 215 km

Segment 2 (Figure 16) is of the 55 – 215 km of the TN272 seismic profile. The bathymetry shows the area is dotted with numerous smaller seamounts with the seismic track passing over the flanks of two seamounts at 65 and 95 km and directly over a seamount at 110 km. From 55 km to the seamount at 110 km there is a thick Unit 1 layer, but Units 2 – 4 are not easily discerned. There is a thick opaque layer of highly disturbed and discontinuous reflectors alternating with sections of chaotic facies. The 10 km contains a lower transparent unit somewhat similar to Unit 3, but it is highly disturbed. The previously clear horizon C is also absent. North of the seamount, the highly disturbed facies continues but some lower sills are visible and at the termination of S_{13} the facies abruptly changes with both the upper layers becoming continuous and the lower Unit 3 layer also visible. North of S_{14}, bedding planes are more clearly defined, and deeper Unit 4 sediments are visible. The sedimentary units continue until terminating at another seamount at 200 km where Unit 2 and part of Unit 3 thin and appear to onlap the seamount. Also, along this segment the Unit 2 – Unit 3 interface has a number of unconformable undulations. Basement is at nearly 7.6 s and then follows the sediments, gradually sloping upwards to 7.3 s.

The section from 55 – 90 km and book-ended by seamounts shows acoustic basement at 7.5s. The basement is interpreted as being Cretaceous intrusions which are overlying more sediments below. There is depth continuity with the gently sloping basement from Segment 1 which is interpreted as Cretaceous, and discontinuity with the sediments and basement depth after the seamount at 110 km. It seems unlikely that there would be such a rapid decrease in sediment thickness. This interpretation also agrees which was previously shown in the regional velocity model from Feng (2016). The visible basement below the sediments after the 110 km seamount, from 140 – 210 km, is interpreted as "true" basement rock of Jurassic age.

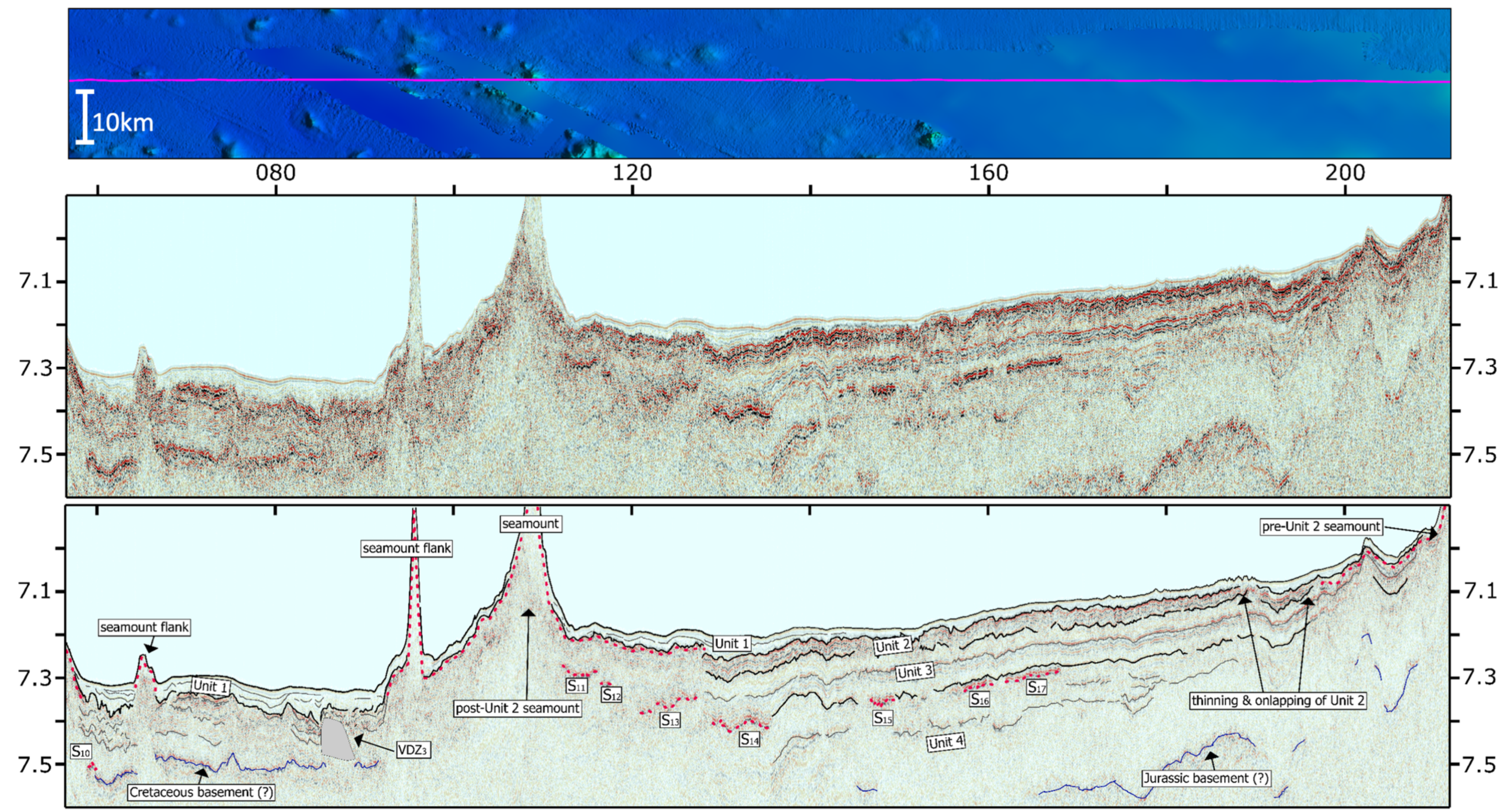

Figure 16.Segment 2 of TN272 seismic line. Above: Local bathymetry in meters (m) along TN272 seismic line (pink). Below: Original and annotated reflection seismic profile with two-way-traveltime (TWT) on the vertical axis in seconds (s) and distance in kilometers

There are eight identified sills within this segment, S_{10}-S_{17}, all of them flat lying or layer parallel. S_{10} directly overlies basement rock, and the sediments above have folded and faulted (Figure 17A). In addition, there is a narrow VDZ that extends upward from the basement and is interpreted as a possible volcanogenic vent. North of S_{10} is VDZ_3 at 85 km (Figure 17B). The surrounding sedimentary layers terminate immediately all the way to basement and there are many diffractive artifacts present in the data. The lack of sediment uplift or volcanogenic vents above indicate it might be the buried edge of seamount flank which can't be seen in the local bathymetry grid as there is no off-line, high-resolution data at this point. The seamount at 110 km appears to have intruded post Unit 2 as the Unit does not onlap the seamount flank, as does Cenozoic Unit 1. The shallower sills S_9, S_{10}, and S_{11}, disturb overlying sediments from 110-130 km over the same interval that the facies change from chaotic to continuous.

Figure 17C shows an unconformable surface between Unit 2 and 3 and a pair of sediment mounds in Unit 3 but seem unrelated to any observed volcanism. Unit 4 is very thick at this point and some stratigraphic reflectors are visible. The thinning and onlapping of Unit 2 and part of Unit 3 on the flank of the seamount at 210 km, indicate that the seamount intruded pre-Unit 2.

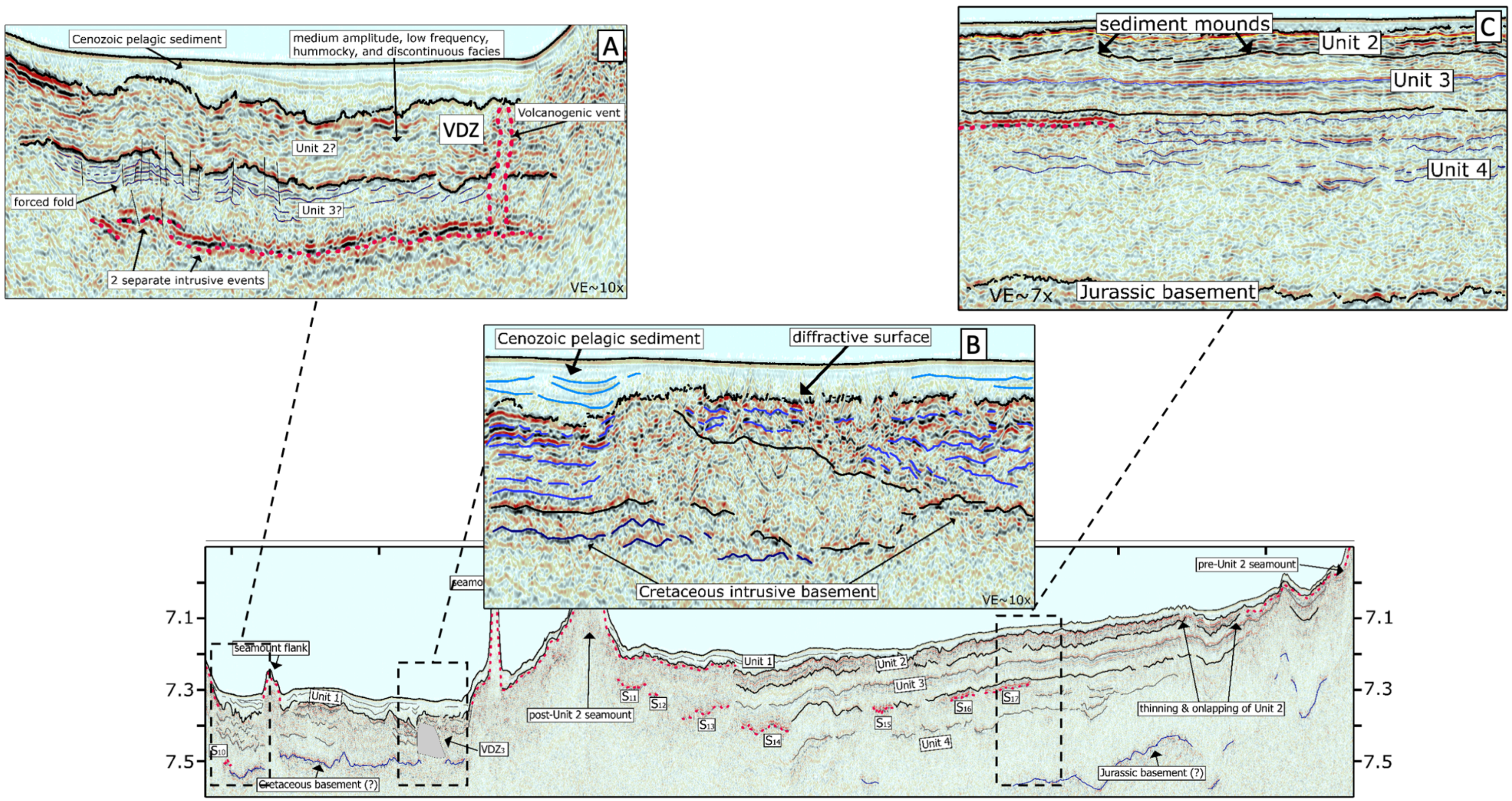

Figure 17.Series of close-ups of segment 2 showing (A) forced folding and a volcanigenic vent, (B) possible buried small seamount flank, (C) a sill intruding a thick sedimentary section (Amplitude scale is the same as in Figure 8)

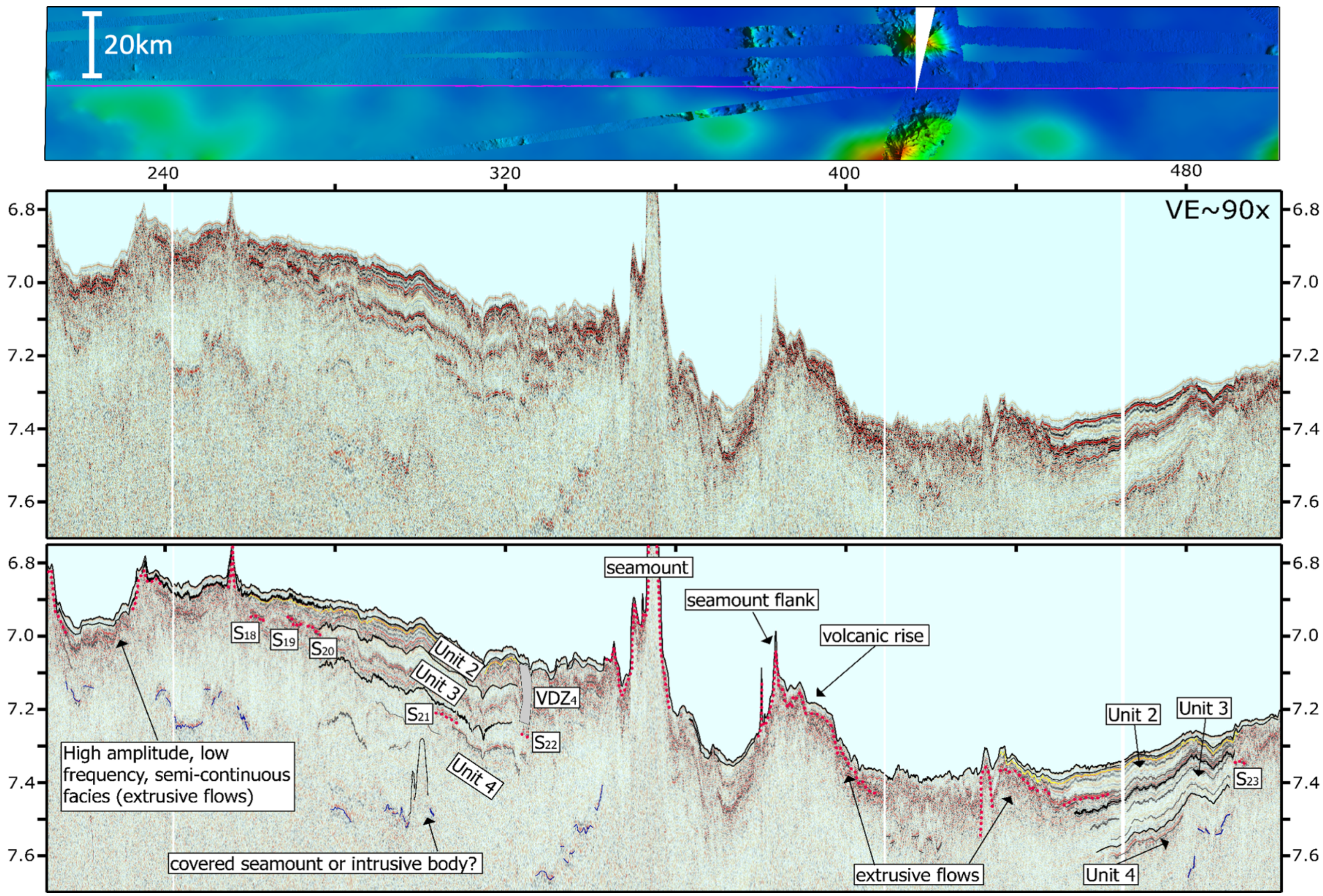

Figure 18. Segment 3 of TN272 seismic line. Above: Local bathymetry in meters (m) along TN272 seismic line (pink). Below: Original and annotated reflection seismic profile with two-way-traveltime (TWT) on the vertical axis in seconds (s) and distance in kilometers (km) on the horizontal axis. See Figure 14 for the annotation legend. Seismic amplitude scale is the same as in Figure 8. Bathymetry scale is the same as Figure 11

Segment 3, 215 – 500 km

Segment 3 encompasses the 215 – 500 km points of the TN272 seismic profile. Bathymetry data (Figure 18) show that the seismic line crosses the flank of a low, broad seamount from 230-250 km, a seamount at 350 km, and a volcanic rise and seamount associated with a linear seamount ridge at 380 km. The seismic data show a new facies at 200 – 230, 390 – 410, and 440 – 460 km. The facies is characterized by very high amplitude, low frequency reflectors that are semi-continuous and strongly attenuate the seismic signal. This facies differs from the sill facies in that there are multiple reflectors, not as continuous as the sills, and they are shallow, only covered by a thin Unit 1. These features are interpreted as buried extrusive flows. There are 6 interpreted sills, all of which are flat lying or layer parallel and none of which disrupt or fold the sediments above. While this segment is interpreted as an area of heavy volcanism evidenced by the appearance of extrusive facies, it also has two sections of thick sediments from 275-325 km and 445-490 km where Units 1-4 are visible (Figure 19). The 445-490 section of sediments does not have any sills and as a result all the units display continuous, parallel facies, with no disruptions. Basement is only visible sporadically across the segment starting at 7.2s and ending at 7.6s. At 300 km there is a mound structure extending up from the basement into Unit 4. It does not cause any folding or disruption of the sediments above and some faint reflectors appear to onlap the structure and therefore is interpreted as a buried seamount.

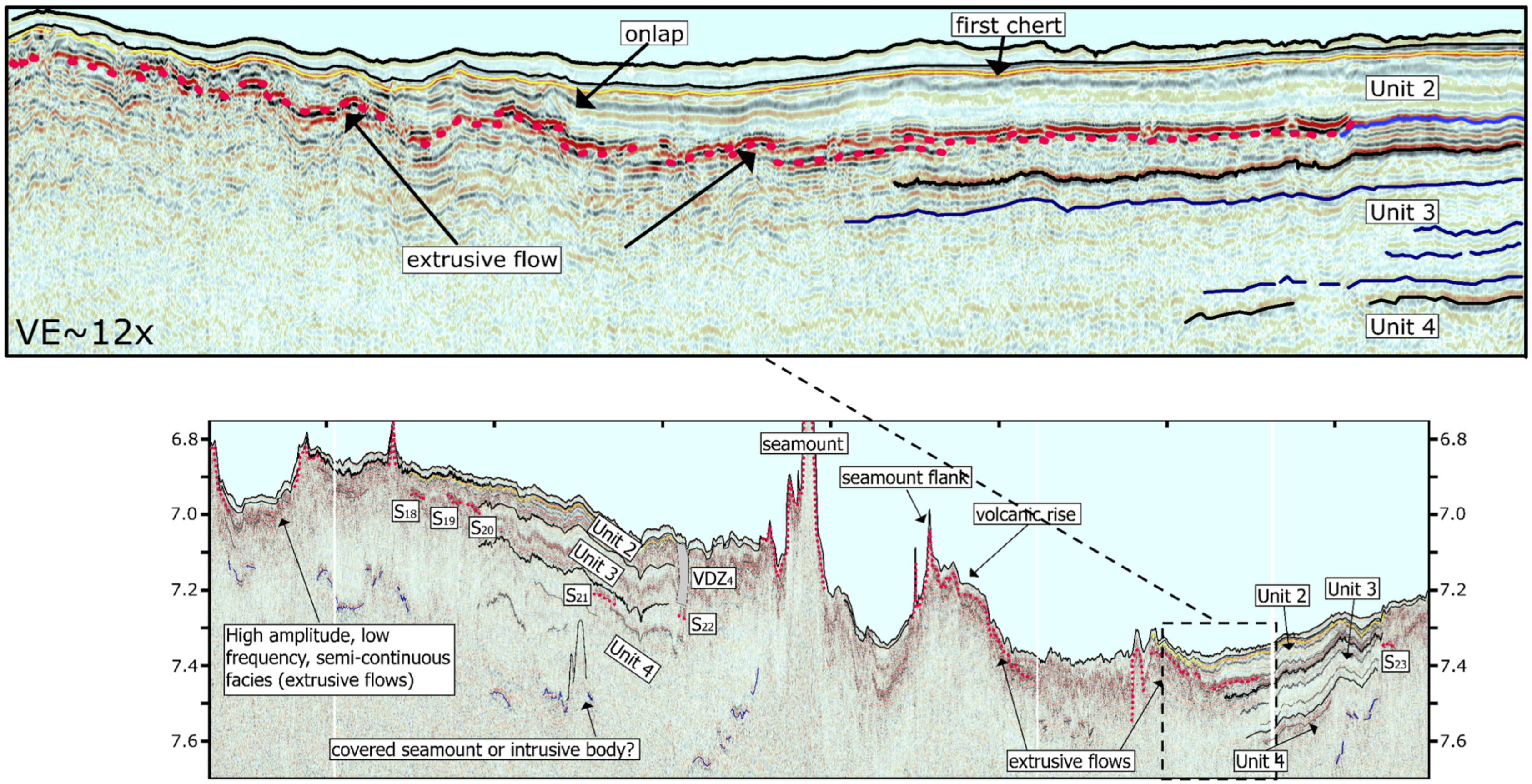

Figure 19. Close-up of a section of segment 3 showing thick sediments and an extrusive flow. Seismic amplitude scale is the same as Figure 8.

Segment 4, 500 – 650 km

Bathymetry along Segment 4 (Figure 20) begins at a local high at 500 km as the survey line crosses the northern flank of a seamount to the south. This is followed by a gentle down slope towards the north. From 510 – 540 km there is a single sequence of multiple high amplitude, low frequency, discontinuous reflectors that is interpreted as an extrusive flow. At 550 km some of the high amplitude reflectors of this facies fall under the criteria for a sill, but they are interpreted as being a continuation of the extrusive flow and the gaps between reflectors interpreted as areas where the flow is out of the plane of the seismic profile. Below the extrusive flow are two interpreted sills, S_{26} and S_{27}. North of the extrusive flow, at 570 km, Units 2, 3, and 4 can be clearly identified.

From 580 – 590 km just below Unit 3 there are two features with sill like signatures. They appear as mounded structures, one with a disturbed zone (VDZ_5) above it. They are both interpreted as laccoliths and VDZ5 is interpreted as a volcanogenic vent with disrupted and folded sedimentary layers. Farther north, VDZ_6 – VDZ_8 are identified at 600 – 620 km and VDZ_9 at 645 km. All of them have low amplitude, chaotic internal reflections, they fold and uplift the sediments above them, and except for VDZ_6, extend all the way down to visible basement. The fact that basement is still visible below makes it unlikely for them to be structures of igneous rock. A large sill (S_{28}) is interpreted north of VDZ_8, below which basement cannot be seen. From 620 – 650 km Units 2-4 are visible but with the difference that Horizon C is missing from Unit 2.

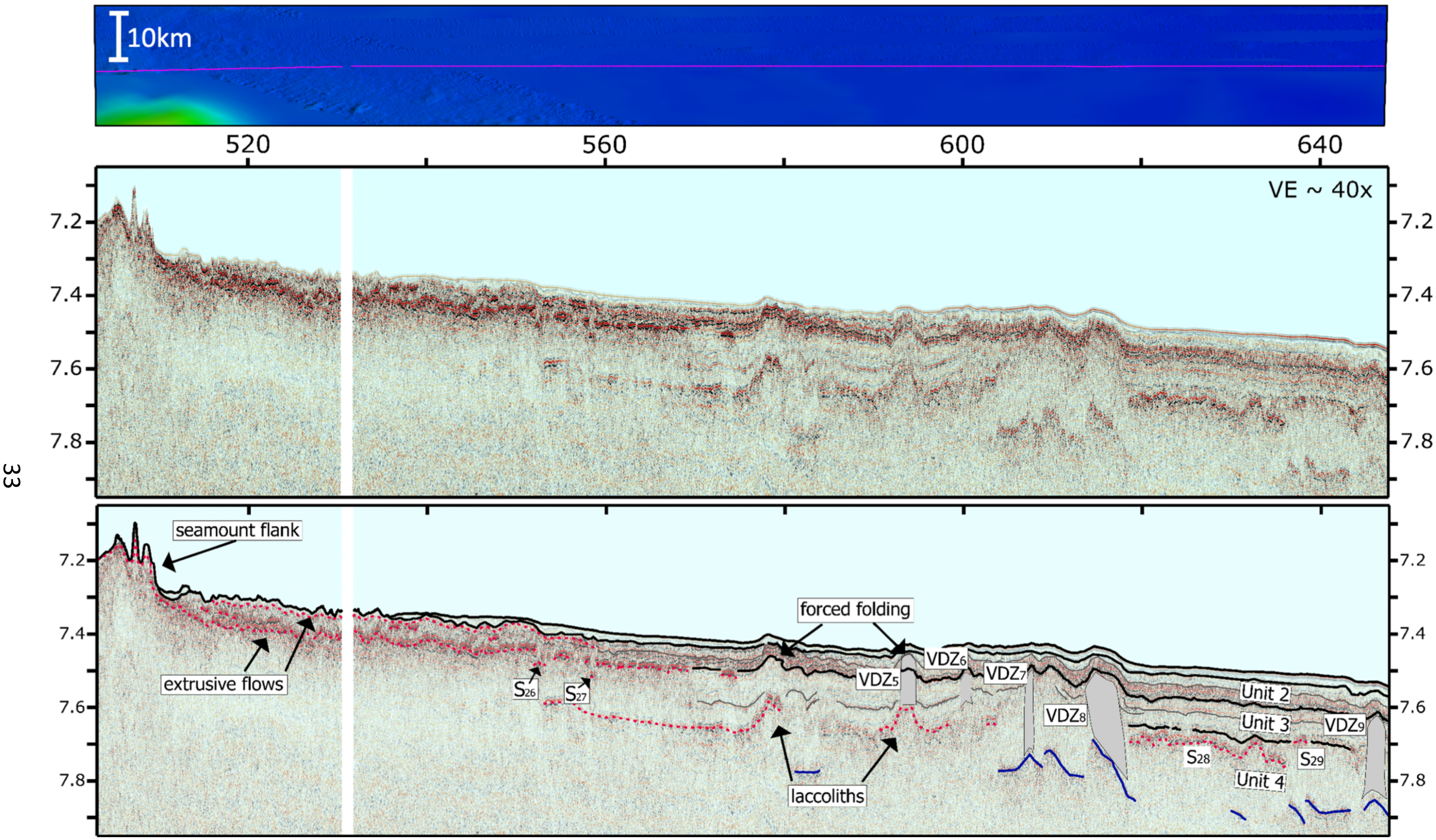

Figure 20. Segment 4 of TN272 seismic line. Above: Local bathymetry in meters (m) along TN272 seismic line (pink). Below: Original and annotated reflection seismic profile with two-way-traveltime (TWT) on the vertical axis in seconds (s) and distance in kilometers (km) on the horizontal axis. See Figure 14 for the annotation legend. Seismic amplitude scale is the same as in Figure 8. Bathymetry scale is the same as Figure 11.

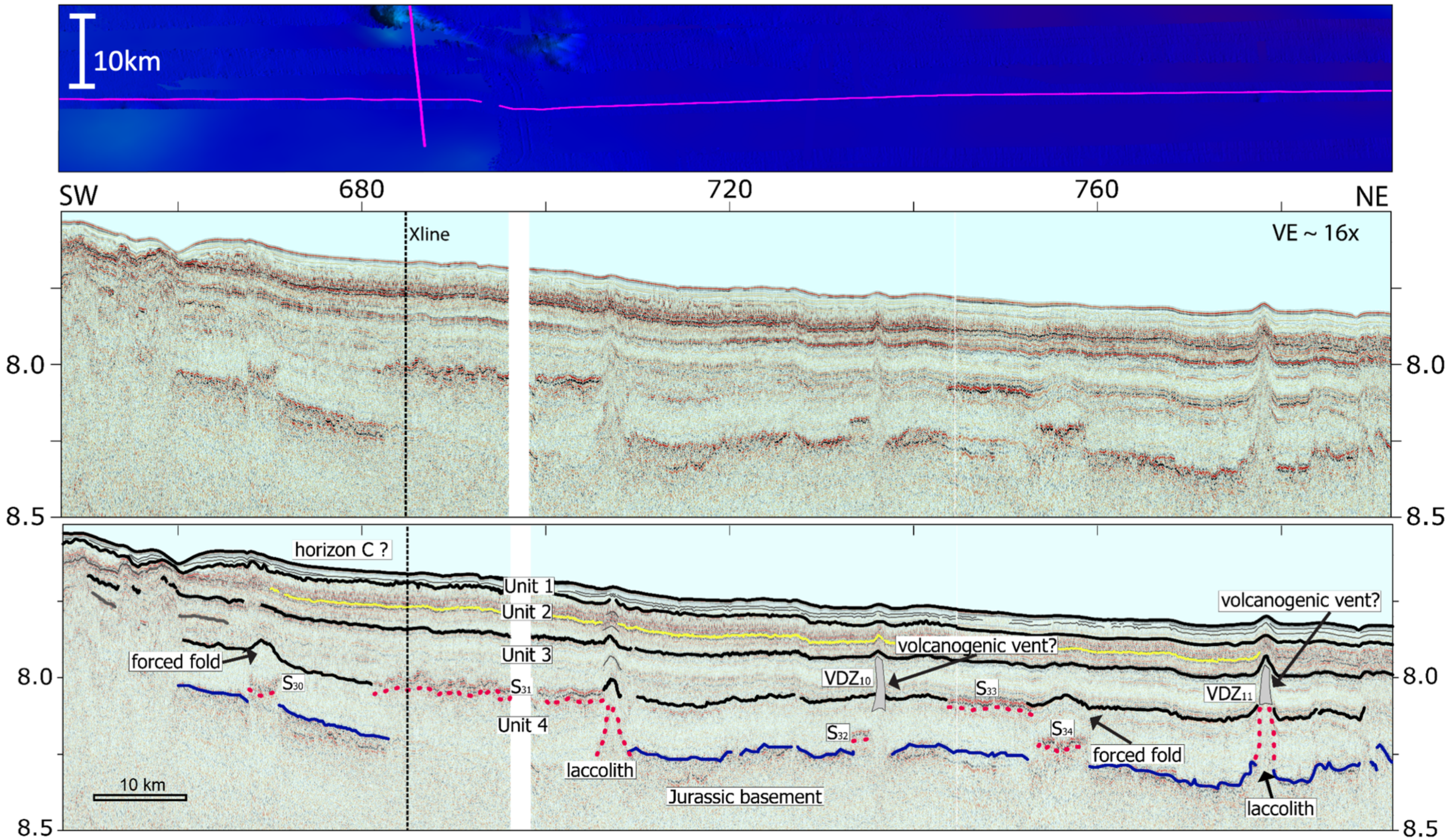

Figure 21. Segment 5 of TN272 seismic line. Above: Local bathymetry in meters (m) along TN272 seismic line (pink). Below: Original and annotated reflection seismic profile with two-way-traveltime (TWT) on the vertical axis in seconds (s) and distance in kilometers (km) on the horizontal axis. See Figure 14 for the annotation legend. Seismic amplitude scale is the same as in Figure 8. Bathymetry scale is the same as Figure 11.

Segment 5, northeast basin, 650 – 800 km

Segment 5 begins at 650 km (Figure 21). There is a bathymetric trough from 650 – 665 km; a result of the survey passing over a moat next to a small flat seamount mound. After this trough the bathymetry remains relatively flat and slopes gently northward to the end of the line. Local bathymetry grid data show that this part of the seismic line has the least amount of surface volcanism and this is reflected in the clarity of the sediments and basement layer. A crossline at 683 km crosses the flank of a seamount northwest of the main line. Basement starts at 8.0 s and then levels off at 8.3 s. Unit 1 is consistently thicker than any other point along the profile and the internal reflectors of Unit 2 are more discontinuous than in Pigafetta Basin.

Five sills are observed in this segment, all of which are flat lying or layer parallel. S_{30} and S_{34} both forced significant sediment folds above them, but those folds only extended partially into Unit 3, indicating they are older than Unit 2 and a subset of Unit 3. S_{31} did not fit the criteria in some aspects in that it has a weaker amplitude than most other interpreted sills and the reflector is rough and discontinuous. It does however, terminate very abruptly and stands out from the surrounding sediment. When looking at the crossline (Figure 22A) S_{31} extends ~10 km to the northwest until it terminates at the seamount. On this crossline, it is the deepest reflector, but as it is clear on the main line that this reflector is a sill overlying basement below, it can be inferred that the basement on the crossline is Cretaceous. On the main line, S_{31} extends to the northeast till it terminates at a mound-shaped laccolith rising from the basement layer at 705 km. This laccolith appears to be similar age to S_{30} and S_{34}. The flanks are visible extending from the basement rock and uplifting sediments in the lowest part of Unit 3, but this uplift decreases significantly at shallower depths and the sediment reflectors are continuous. VDZs 10 and 11 are both interpreted as being volcanogenic vents. For VDZ_{10} the vent system is connected to the S_{32} sill and VDZ_{11} is a vent above a laccolith mound.

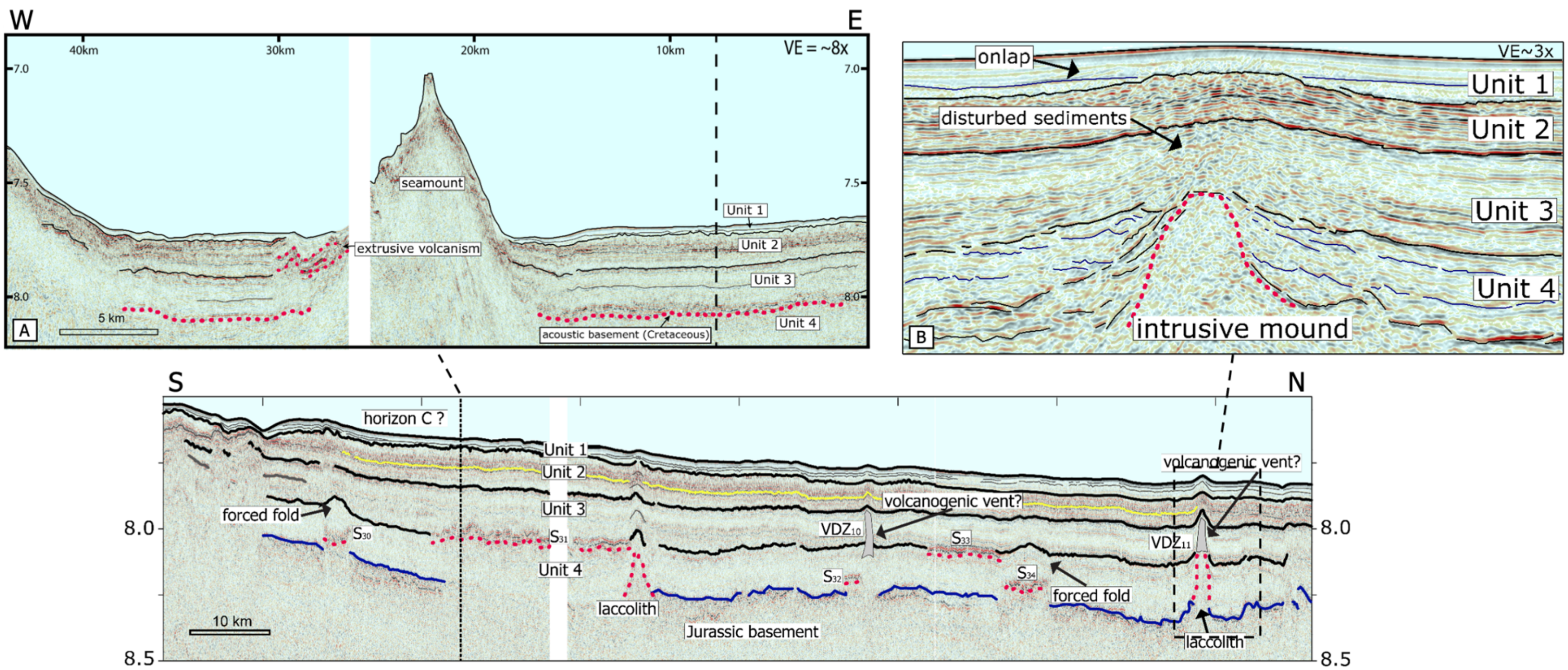

Figure 22. (A) Crossline associated with segment 5 (B) Close-up of segment 5 laccolith. (amplitude scales as in Figure 8)

5. DISCUSSION

Sedimentary layers

It is reasonable to assume that the sediments mapped on TN272 are similar to those observed at ODP Sites 800 and 801 as these drill sites are not far away and in the case of Site 801, the data are from the same basin. The biggest difference is that the SW end of TN272 seismic line does not sample an area of Pigafetta basin as deep as Site 801 and is in an area of greater volcanism. Unit 1 is most likely the same brown pelagic clay seen at Sites 800 and 801, which was dated to be from the present back to the late Campanian (Table 1). Unit 2 is probably the same hard chert and porcellanite layer although there is possibly some lithological difference in the northern basin where the NE end no longer has a clear Horizon C. Unit 3, which is a volcaniclastic layer with some pelagic intervals at the ODP sites, is the layer differing the most from the TN272 seismic line in terms of thickness; however, the seismic thicknesses are not well constrained. The boundary between Unit 3 and 4 on the seismic line was based on the traveltime at which the facies changed to one characterized by only chaotic reflectors and was often unclear. The Unit 4 observed at Site 801 had a strong reflector at the top of the unit and did contain some continuous internal reflectors as well. It is unclear if the chaotic character of the facies is due to the physical characteristics of the sedimentary rock. It is possible that the chaotic character is due to a weaker source being unable to image Unit 4 properly, most notably in Segments 2 and 3 where Unit 4 thickness is greatest. With the boundary between Unit 3 and 4 not well constrained in the TN272 seismic, it is possible a volcaniclastic lithology extends deeper into parts of the TN272 Unit 4.

When comparing the apparent sediment thicknesses of the SW Pigafetta Basin and northeast basin of TN272 the NE end appears to be thicker. The main reason for this is the SW end sediments are invaded by sills to a much greater degree. There was very little Unit 4 sediment observed in SW end, and this combined with the refraction velocity model data and the depth to basement at Sites 800 and 801 (Table 1), indicates that the SW end is completely covered in thick Cretaceous sills.

Sill geometries and other igneous bodies.

Of the 34 identified sills in the seismic profile, all of them have flat-lying or layer-parallel geometries with very little apparent cross-cutting of sedimentary layers. There is some limited evidence from other seismic observations of sills, which are mostly in sedimentary basins, showing that layer parallel geometries are more commonly found at very shallow emplacement depths (<500m) than other geometries (Jackson *et al*., 2013; Magee *et al*., 2014; Mark *et al*., 2015). Experimental studies show that this is a result of mechanical properties of shallow unconsolidated sediments, in which intrusions usually display a magma finger geometry rather than saucer-shaped geometry (Schofield *et al*., 2012; Magee *et al*., 2019, Poppe *et al*., 2019). Saucer shaped sills can form at relatively shallow depths, <1000m (Jackson *et al*., 2013; Magee *et al*., 2014; Mark *et al*., 2015), but require sediments to be consolidated and have strength (Galland *et al*. 2009, Schmiedel *et al*., 2017). In addition to the host rock, the viscosity, flux, and size of the magma source is a factor in sill geometry, and in the case of layer parallel sills, the rigidity contrasts between host rock layers is also a factor (Kavanaugh *et al*., 2006).

Most sills on the seismic line were emplaced at one of two levels in the sedimentary sections. One is at the horizon defining the boundary between Units 3 and 4, and the other is at the base of Unit 4, directly overlying basement. The consistent emplacement at those levels suggests a set of physical parameters that is constant throughout the area. The base of Unit 3 which is primarily volcaniclastics, may explain this as volcaniclastics are among the mechanically weakest sediments (Frolova. 2008).

After sills, the next most common feature observed are intrusive laccolith mounds (Figures 13, 19, 20). They are characterized by chaotic facies and vertically crosscut the sedimentary layers. They are believed to be intrusive due to the presence of mounded sediments above them and the lack of onlapping sediments on their flanks, although at times it is difficult to discern the structure with certainty because most of the mounds are in Unit 4 where little sedimentary layering is visible. It also might be expected that igneous intrusive bodies should display a hard reflector as is the case with the laccolith example in Figure 6D. However, when looking at most of the extrusive igneous seamounts along the seismic profile, they also do not display a strong impedance contrast, due to the quality of the data and issues with imaging steeply dipping structures. These issues extend to intrusive mounds as well.

Forced folding and disturbed sediments above igneous features

All of the intrusive mounds in the seismic profile affect the surrounding sediment by causing forced folding of the sedimentary layers above the intrusion. Most of the sills show little to no forced folding but there are a few examples that do: sills S_9 (Figure 14), S_{10} (Figure 16), S_{30}, and S_{34} (Figure 21). Forced folding can be used to date the intrusion and it is evident that both S_{26} and S_{30} formed midway during Unit 3 where the folding ends.

Forced folding has been documented in sedimentary basins above saucer-shaped sills and is thought to form through (1) differential compaction where the fold is formed post-intrusion from sediment compacting less above an intrusive body than adjacent sediments with no intrusion below, and/or (2) intrusion induced uplift in which the sediments fold as a direct result of the pressure from the intruding body and consequent elastic bending of the overburden and is followed by sediment onlap around the fold (Hansen and Cartwright, 2006; Jackson *et al*., 2013; Magee *et al*., 2019). The latter process seems more likely for sills observed in the seismic profile because of the shallow emplacement of the igneous features and low compaction at shallow depths. The laccolith mound in Figure 22B with onlapping sediments above demonstrates this. The lack of folding above most of the sills is also probably due to the shallow emplacement depth and lack of sediment consolidation. Einsele *et al*. (1980) show an example of deep ocean sediments being intruded by magma at shallow depths (<300m) and leading to rapid ejection of pore fluids from the host rock. They argue that the fluid removal creates enough space for the intruding magma to not cause any apparent folding in the overlying sediments. In addition, Einsele *et al*. (1980) observed volcanogenic vent systems above the sills due to the fluid removal, a phenomenon observed on the TN272 seismic profile. The seismic interpretation of the volcanogenic vents is a hypothesis based on studies using 3D seismic data where there is a high correspondence of mound structures forming above sills and which suggests a causal connection between the sills and the mounds. That connection is reinforced by the observation of chaotic and disrupted reflection chimneys often with increased impedance contrast (Davies *et al.*, 2002; Holford *et al.*, 2017; Jackson, 2012; Magee *et al.,* 2015b; Planke *et al.*, 2005; Reynolds *et al.*, 2016; Sun *et al.*, 2019). Figures 13 and 20 show examples of large paleo-volcanogenic vent systems that extend almost to the surface, but many of the sills observed have highly disturbed sediments above them that are most likely also smaller volcanogenic vent systems as a result of this rapid fluid ejection (e.g., sills S_1 and S_5, Figure 14).

Regional Cretaceous volcanism in the WPSP

The evidence from the igneous features that display forced folding suggests that the much of the volcanism along the seismic profile occurred during Unit 2 deposition, which if extended to ODP Sites 800 and 801, would date the volcanism to the Late Cretaceous, from 72-94 Ma (Table 1). This agrees with the ages for the primary seamounts in the area (Figure 3). The similar age to the surrounding seamounts also suggests that the intrusions were formed from the same anomaly which formed the primary seamounts. Stadler and Tominaga (2015) saw no apparent lineation or grouping of the secondary volcanic features in Western Pigafetta Basin from interpretation of the MTr and FM35-12 seismic profiles, and they also concluded that these secondary features are the same age as the primary seamounts. These observations together, they believed, reinforce the idea that the secondary features formed from the same intraplate process as the surrounding primary seamounts. Along the TN272 profile there is a mixture of random and non-random spatial distributions of the secondary and tertiary volcanic features in Pigafetta Basin (Figure 11). The non-random distributions are evidence that there are mechanisms that can cause such distributions even at a small scale and further study is required to understand them and how they are connected to the primary seamounts.

What is certain is that a tremendous amount of melt material was introduced into the crust in this region. The broad regional swell observed in the gravity and bathymetry from 100 – 400 km indicates a large amount of igneous material being introduced into the crust but appears to have formed from a different melt transport process than most of the surrounding primary seamounts. The reflection seismic data indicates that this swell consists of many lateral flows and which appear to be more diffuse than the flows of the surrounding primary seamounts. Whether or not and in what manner the swell was connected with the melt transport of the surrounding seamounts is uncertain.

6. CONCLUSIONS

(1) The primary sedimentary units observed in seismic and ODP sites 800 and 801 in West Pigafetta Basin, can be extended across Pigafetta Basin and past the edges of the WPSP to the northeast, and can be used as a rough estimate for the age of intrusive igneous features.

(2) There are 34 sills and 6 laccoliths along the TN272 seismic line. Based on stratigraphic level of emplacement, these were predominantly emplaced during the Late Cretaceous (72 – 94 Ma).

(3) Intrusive sills in the WPSP display a dominantly layer parallel geometry and are rarely saucer shaped like sills in other sedimentary basins.

(4) Forced folding is rare above sills in WPSP but is displayed more commonly above laccolith mounds. Volcanogenic vent zones and altered sediments are common above both igneous sills and laccoliths.

(5) The Northeast Pigafetta Basin has an abundance of Cretaceous sills which, in places, completely cover Jurassic crust and sediments below.

(6) Significant igneous melt was introduced into the crust in the WPSP through multiple means of transport, and can be expressed as sills and laccoliths, broad surface flows, and acute seamount structures.

BIBLIOGRAPHY

Á Horni, J., Hopper, J. R., Blischke, A., Geisler, W. H., Stewart, M., McDermott, K., Judge, M., Erlendsson, Ö., and Árting, U. (2017). Regional distribution of volcanism within the North Atlantic Igneous Province. *Geological Society, London, Special Publications*, *447*(1), 105–125.

Abrams, L. J., Larson, R. L., Shipley, T. H., and Lancelot, Y. (1992). The seismic stratigraphy and sedimentary history of the East Mariana and Pigafetta Basins of the Western Pacific. *Proceedings of the Ocean Drilling Program, 129 Scientific Results, 129,* 551–569.

Abrams, L. J., Larson, R. L., Shipley, T. H., and Lancelot, Y. (1993). Cretaceous volcanic sequences and Jurassic oceanic crust in the East Mariana and Pigafetta basins of the western Pacific. In Pringle, M.S., Sager, W.W., Sliter, W.V., Stein, S. (Eds.), *The Mesozoic Pacific: Geology, Tectonics, and Volcanism*, *77*, 77–101. American Geophysical Union, Washington D.C.

Anderson, D. L., and Natland, J. H. (2007). Evidence for mantle plumes?. *Nature*, *450*, E15.

Clouard, V., and Bonneville, A. (2005). Ages of seamounts, islands, and plateaus on the Pacific plate. *Special Papers-Geological Society of America*, *388*, 71.

Christeson, G. L., Goff, J. A., and Reece, R. S. (2019). Synthesis of oceanic crustal structure from two-dimensional seismic profiles. *Reviews of Geophysics*, *57*(2), 504–529.

Courtillot, V., Davaille, A., Besse, J., and Stock, J. (2003). Three distinct types of hotspots in the Earth's mantle. *Earth and Planetary Science Letters*, *205*(3–4), 295–308.

Davies, R., Bell, B. R., Cartwright, J. A., and Shoulders, S. (2002). Three-dimensional seismic imaging of Paleogene dike-fed submarine volcanoes from the Northeast Atlantic margin. *Geology (Boulder)*, *30*(3), 223–226.

Einsele, G., Gieskes, J. M., Curray, J., Moore, D. M., Aguayo, E., Aubry, M.-P., Fornari, D., Guerrero, J., Kastner, M., Kelts, K., Lyle, M., Matoba, Y., Molina-Cruz, A., Niemitz, J., Rueda, J., Saunders, A., Schrader, H., Simoneit, B., and Vacquier, V. (1980). Intrusion of basaltic sills into highly porous sediments, and resulting hydrothermal activity. *Nature*, *283*(5746), 441–445.

Feng, H. S.-H. (2016). Seismic constraints on the processes and consequences of secondary igneous evolution of Pacific oceanic lithosphere [Doctoral dissertation, Massachusetts Institute of Technology and Woods Hole Oceanographic Institute]. https://hdl.handle.net/1912/7803

Foulger, G. R. (2007). The "plate" model for the genesis of melting anomalies. In Foulger, G.R. and Jurdy, D.M. (Eds), *Plates, Plumes, and Planetary Processes. 430*. 1–28.

Francis, E. H. (1982). Magma and sediment-I emplacement mechanism of late Carboniferous tholeiite sills in northern Britain. *Journal of the Geological Society*, *139*(1), 1–20.

Frolova, Y.V. (2008). Specific features in the composition, structure, and properties of volcaniclastic rocks. *Moscow University Geology Bulletin, 63*(1), 28–37.

Galland, O., Burchardt, S., Hallot, E., Mourgues, R., and Bulois, C. (2014). Dynamics of dikes versus cone sheets in volcanic systems. *Journal of Geophysical Research: Solid Earth*, *119*(8), 6178–6192.

Gonnermann, H., Taisne, B. (2015) Magma transport in dikes. In Haraldur Sigurdsson (Ed.), *The encyclopedia of volcanoes* (2nd ed., pp 215–224), Academic Press

Handschumacher, D. W., Sager, W. W., Hilde, T. W. C., and Bracey, D. R. (1988). Pre-Cretaceous tectonic evolution of the Pacific plate and extension of the geomagnetic polarity reversal time scale with implications for the origin of the Jurassic "Quiet Zone". *Tectonophysics*, *155*(1–4), 365–380.

Hansen, D. M., and Cartwright, J. (2006). The three-dimensional geometry and growth of forced folds above saucer-shaped igneous sills. *Journal of Structural Geology*, *28*(8), 1520–1535.

Holford, S. P., Schofield, N., and Reynolds, P. (2017). Subsurface fluid flow focused by buried volcanoes in sedimentary basins: Evidence from 3D seismic data, Bass Basin, offshore southeastern Australia. *Interpretation*, 5: SK39–SK50.

Hyndman, D. W., and Alt, D. (1987). Radial dikes, laccoliths, and gelatin models. *The Journal of Geology*, *95*(6), 763–774.

Jackson, C. A.-L. (2012) Seismic reflection imaging and controls on the preservation of ancient sill-fed magmatic vents. *Journal of the Geological Society*, *169*, 503–506.

Jackson, C. A.-L., Schofield, N., and Golenkov, B. (2013). Geometry and controls on the development of igneous sill-related forced folds: A 2-d seismic reflection case study from offshore southern Australia. *Geological Society of America Bulletin*, *125*(11–12), 1874–1890.

Kaneda, K., Kodaira, S., Nishizawa, A., Morishita, T., and Takahashi, N. (2010). Structural evolution of preexisting oceanic crust through intraplate igneous activities in the Marcus-Wake seamount chain. *Geochemistry, Geophysics, Geosystems*, *11*, Q10014.

Kavanagh, J. L., Menand, T., and Sparks, R. S. (2006). An experimental investigation of sill formation and propagation in layered elastic media. *Earth and Planetary Science Letters*, *245*(3–4), 799–813.

Koppers, A. A., Staudigel, H., Pringle, M. S., and Wijbrans, J. R. (2003). Short-lived and discontinuous intraplate volcanism in the South Pacific: Hot spots or extensional volcanism? *Geochemistry, Geophysics, Geosystems*, *4*(10).

Lancelot, Y., Larson, R.L., *et al.* (1990). *Proceedings of the Ocean Drilling Program, Initial Reports*, 129: College Station, TX (Ocean Drilling Program), 91–170.

Lockwood, J. P., and Hazlett, R. W. (2010). *Volcanoes: global perspectives*. John Wiley and Sons.

Magee, C., Jackson, C. A.-L., and Schofield, N. (2014). Diachronous sub-volcanic intrusion along deep-water margins: Insights from the Irish Rockall Basin. *Basin Research*, *26*(1), 85–105.

Magee, C., Maharaj, S. M., Wrona, T., and Jackson, C. A.-L. (2015a). Controls on the expression of igneous intrusions in seismic reflection data. *Geosphere*, *11*(4), 1024–1041.

Magee, C., Duffy, O. B., Purnell, K., Bell, R. E., Jackson, C. A. L., and Reeve, M. T. (2015b). Fault-controlled fluid flow inferred from hydrothermal vents imaged in 3D seismic reflection data, offshore NW Australia. *Basin Research*, *28*(3), 299–318.

Magee, C., Muirhead, J. D., Karvelas, A., Holford, S. P., Jackson, C. A. L., Bastow, I. D., Schofield, N., Stevenson, C. T. E., McLean, C., McCarthy, W., and Shtukert, O. (2016). Lateral magma flow in mafic sill complexes. *Geosphere*, *12*(3), 809–841.

Magee, C., Muirhead, J., Schofield, N., Walker, R. J., Galland, O., Holford, S., Spacapan, J., Jackson, C. A.-L., and McCarthy, W. (2019). Structural signatures of igneous sheet intrusion propagation. *Journal of Structural Geology*, *125*, 148–154.

Malthe-Sørenssen, A., Planke, S., Svensen, H., and Jamtveit, B. (2004). Formation of saucer-shaped sills. *Geological Society, London, Special Publications*, *234*(1), 215–227.

Mark, N. J., Holford, S. P., Schofield, N., Eide, C. H., Pugliese, S., Watson, D. A., and Muirhead, D. (2019). Structural and lithological controls on the architecture of igneous Intrusions: Examples from the NW Australian shelf. *Petroleum Geoscience*, *26*(1), 50–69.

Mitchum, R. M., Vail, P.R., and Sangree, J.B. (1977) Seismic stratigraphy and global changes of sea level: Part 6. Stratigraphic interpretation of seismic reflection patterns in depositional sequences: Section 2. Application of seismic reflection configuration to stratigraphic interpretation. In Payton, C.E. (Ed), *Seismic Stratigraphy—Applications to Hydrocarbon Exploration*, 117 – 133.

Morgan, W. J. (1971). Convection Plumes in the Lower Mantle. *Nature*, *230*(5288), 42–43.

Müller, R. D., Sdrolias, M., Gaina, C., and Roest, W. R. (2008). Age, spreading rates, and spreading asymmetry of the world's ocean crust. *Geochemistry, Geophysics, Geosystems*, *9*(4).

Plank, T., Ludden, J.N., Escutia C., *et al*. (2000). *Proceedings of the Ocean Drilling Program, Initial Reports.*, *185*: College Station, TX (Ocean Drilling Program)

Planke, S., Millett, J. M., Maharjan, D., Jerram, D. A., Abdelmalak, M. M., Groth, A., Hoffmann, J., Berndt, C., and Myklebust, R. (2017). Igneous seismic geomorphology of buried lava fields and coastal escarpments on the Vøring volcanic rifted margin. *Interpretation*, *5*(3).

Planke, S., Rasmussen, T., Rey, S. S., and Myklebust, R. (2005). Seismic characteristics and distribution of volcanic intrusions and hydrothermal vent complexes in the Vøring and Møre Basins. *Geological Society, London, Petroleum Geology Conference Series*, *6*(1), 833–844.

Planke, S., Symonds, P. A., Alvestad, E., and Skogseid, J. (2000). Seismic volcanostratigraphy of large-volume basaltic extrusive complexes on rifted margins. *Journal of Geophysical Research: Solid Earth*, *105*(B8), 19335–19351.

Poppe, S., Holohan, E. P., Galland, O., Buls, N., Van Gompel, G., Keelson, B., Tournigand, P.-Y., Brancart, J., Hollis, D., Nila, A., and Kervyn, M. (2019). An inside perspective on magma intrusion: Quantifying 3d displacement and strain in laboratory experiments by dynamic x-ray computed tomography. *Frontiers in Earth Science*, *7*.

Premoli Silva, I., Haggerty, J., Rack, F., et al., 1993. *Proceedings of the Ocean Drilling Program, Initial Reports.*, 144: College Station, TX (Ocean Drilling Program).

Rea, D. K., and Leinen, M. (1986). Crustal subsidence and Calcite deposition in the South Pacific Ocean. *Initial Reports of the Deep Sea Drilling Project*, *92*, 299–303.

Rea, D. K., and Lyle, M. W. (2005). Paleogene calcite compensation depth in the eastern subtropical Pacific: Answers and questions. *Paleoceanography*, *20*(1).

Reynolds, P., Schofield, N., Brown, R. J., and Holford, S. P. (2017). The architecture of submarine monogenetic volcanoes - insights from 3D seismic data. *Basin Research*, *30*, 437–451.

Sandwell, D. T., Müller, R. D., Smith, W. H., Garcia, E., and Francis, R. (2014). New global marine gravity model from Cryosat-2 and Jason-1 reveals buried tectonic structure. *Science*, *346*(6205), 65–67.

Schmiedel, T., Galland, O., and Breitkreuz, C. (2017). Dynamics of sill And Laccolith Emplacement in the brittle Crust: Role of host Rock strength and deformation mode. *Journal of Geophysical Research: Solid Earth*, *122*(11), 8860–8871.

Schofield, N. J., Brown, D. J., Magee, C., and Stevenson, C. T. (2012). Sill morphology and comparison of brittle and non-brittle emplacement mechanisms. *Journal of the Geological Society*, *169*(2), 127–141.

Stadler, T. J., and Tominaga, M. (2015). Intraplate volcanism of the western Pacific: New insights from geological and geophysical observations in the Pigafetta Basin. *Geochemistry, Geophysics, Geosystems*, *16*(9), 3015–3033.

Sun, Q., Jackson, C. A.-L., Magee, C., Mitchell, S. J., and Xie, X. (2019). Extrusion dynamics of deepwater volcanoes revealed by 3-D seismic data. *Solid Earth*, *10*(4), 1269–1282.

Thomson, K., and Hutton, D. (2004). Geometry and growth of sill complexes: Insights using 3D Seismic from the North Rockall Trough. *Bulletin of Volcanology*, *66*(4), 364–375.

Tominaga, M., Tivey, M. A., and Sager, W. W. (2015). Nature of the Jurassic Magnetic Quiet Zone. *Geophysical Research Letters*, *42*(20), 8367–8372.

Torsvik, T. H., Steinberger, B., Shephard, G. E., Doubrovine, P. V., Gaina, C., Domeier, M., Conrad, C. P., and Sager, W. W. (2019). Pacific-Panthalassic reconstructions: Overview, errata and the way forward. *Geochemistry, Geophysics, Geosystems*, *20*(7), 3659–3689.

Tozer, B., Sandwell, D. T., Smith, W. H., Olson, C., Beale, J. R., and Wessel, P. (2019). Global bathymetry and topography at 15 Arc SEC: SRTM15+. *Earth and Space Science*, *6*(10), 1847–1864.

Van Andel, T. H. (1975). Mesozoic/Cenozoic calcite compensation depth and the global distribution of calcareous sediments. *Earth and Planetary Science Letters*, *26*(2), 187–194.

Van Avendonk, H. J., Davis, J. K., Harding, J. L., and Lawver, L. A. (2017). Decrease in oceanic crustal thickness since the breakup of Pangaea. *Nature Geoscience*, *10*(1), 58–61.

Walker, F., Schofield, N., Millett, J., Jolley, D., Holford, S., Planke, S., Jerram, D. A., and Myklebust, R. (2020). Inside the volcano: Three-dimensional magmatic architecture of a buried shield volcano. *Geology*, *49*(3), 243–247.

White, J.L., Sparks, R. S. J., Bailey, K., Barnett, W. P., Field, M., Windsor, L. (2012). Kimberlite sills and dykes associated with the Wesselton Kimberlite Pipe, Kimberley, South Africa. *South African Journal of Geology, 115*(1), 1–32.

Wilson, J. T. (1963). A possible origin of the Hawaiian Islands. *Canadian Journal of Physics*, *41*(6), 863–870.

Yan, Q., Milan, L., Saunders, J. E., and Shi, X. (2021). Petrogenesis of basaltic lavas from the West Pacific Seamount Province: Geochemical and Sr-Nd-Pb-Hf Isotopic Constraints. *Journal of Geophysical Research: Solid Earth*, *126*(5).